Swart, P.K., Eberli, G.P., Malone, M.J., and Sarg, J.F. (Eds.), 2000
Proceedings of the Ocean Drilling Program, Scientific Results, Vol. 166

17. OVERVIEW OF INTERSTITIAL FLUID AND SEDIMENT GEOCHEMISTRY, SITES 1003–1007 (BAHAMAS TRANSECT)[1]

Philip A. Kramer,[2] Peter K. Swart,[2] Eric H. De Carlo,[3] and Neils H. Schovsbo[4]

ABSTRACT

A review of interstitial water samples collected from Sites 1003–1007 of the Bahamas Transect along with a shore-based analysis of oxygen and carbon isotopes, minor and trace elements, and sediment chemistry are presented. Results indicate that the pore-fluid profiles in the upper 100 meters below seafloor (mbsf) are marked by shifts between 20 and 40 mbsf that are thought to be caused by changes in sediment reactivity, sedimentation rates, and the influence of strong bottom currents that have been active since the late Pliocene. Pore-fluid profiles in the lower Pliocene–Miocene sequences are dominated by diffusion and do not show significant evidence of subsurface advective flow. Deeper interstitial waters are believed to be the in situ fluids that have evolved through interaction with sediments and diffusion.

Pore-fluid chemistry is strongly influenced by carbonate recrystallization processes. Increases in pore-fluid Cl^- and Na^+ with depth are interpreted to result mainly from carbonate remineralization reactions that are most active near the platform margin. A lateral gradient in detrital clay content observed along the transect, leads to an overall lower carbonate reactivity, and enhances preservation of metastable aragonite further away from the platform margin. Later stage burial diagenesis occurs at slow rates and is limited by the supply of reactive elements through diffusion.

INTRODUCTION

A primary goal of Ocean Drilling Program (ODP) Leg 166 was to examine fluid flow and carbonate diagenesis associated with the carbonate platform margin. Investigations of the pore-fluid geochemistry are useful in setting limits on the degree of diagenesis and fluid movement based on the magnitude and shape of pore-fluid profiles (Kastner et al., 1990; Swart et al., 1993; Gieskes et al., 1993). Sites 1003–1007 of Leg 166 were drilled through periplatform carbonate sediments along an off-bank transect adjacent to the western margin of the Great Bahama Bank in the Santaren Channel (Fig. 1). The five sites span a distance of 25 km with water depths ranging from 350 m at the most proximal site (Site 1005) to 658 m at the distal site (Site 1006). The deepest site (Hole 1007C) penetrated upper Oligocene sediments at a depth of 1238 meters below seafloor (mbsf). Sites 1003–1007 were drilled along an extension of a Western Geophysical seismic line, which extends from the Great Bahama Bank into the Straights of Florida (Eberli, Swart, Malone, et al., 1997). The remarkable continuity of the sedimentary sequences from the proximal to the distal sites allows for a detailed correlation of the pore-fluid chemistry profiles. In addition, the depth to which pore fluids were collected through semilithified sediments provides a particularly good data set for understanding large-scale hydrogeochemical processes within a carbonate platform margin.

The objective of this paper is to synthesize shipboard pore-fluid results for the Bahamas Transect and to integrate them with trace element and oxygen stable isotope data presented in DeCarlo and Kramer (Chap. 9, this volume) and Swart (Chap. 8, this volume). Results from solid-phase minor and trace element data for Sites 1007 and 1005 are also presented along with stable $\delta^{13}C$ data from pore-fluid dissolved inorganic carbon (DIC). An emphasis is placed on discussing fluid flow and other diagenetic processes highlighted by the pore-fluid chemistry.

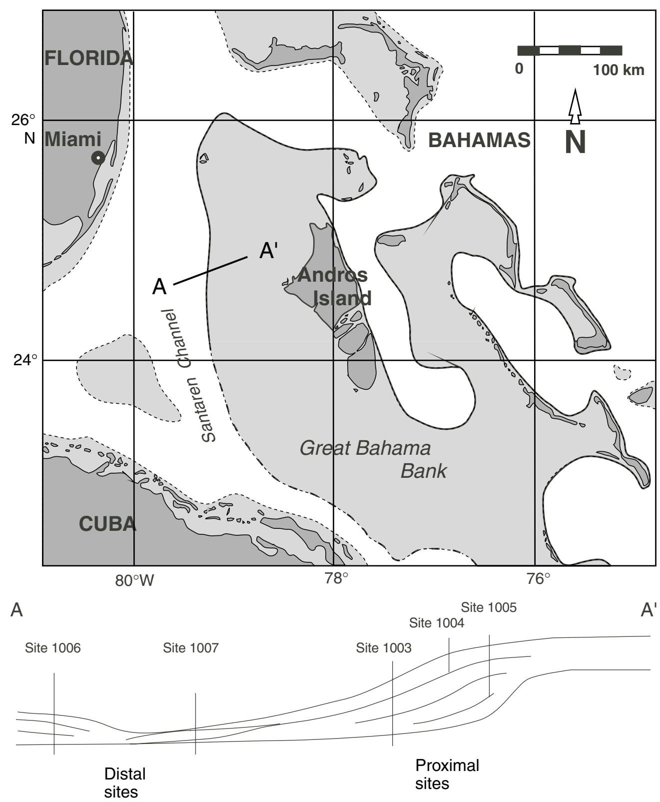

Figure 1. Location of sites drilled during Leg 166 along the Bahamas Transect superimposed on a schematic cross-section of the study area.

Sequence Stratigraphic Framework

A solid sequence stratigraphic framework is important for understanding and interpreting pore-fluid chemistry profiles.

[1]Swart, P.K., Eberli, G.P., Malone, M.J., and Sarg, J.F. (Eds.), 2000. *Proc. ODP, Sci. Results,* 166: College Station TX (Ocean Drilling Program).

[2]Department of Marine Geology and Geophysics, Rosenstiel School of Marine and Atmospheric Science, University of Miami, 4600 Rickenbacker Causeway, Miami FL 33149, USA. Correspondence author: PKramer@RSMAS.MIAMI.EDU

[3]Department of Oceanography, SOEST, 1000 Pope Road, University of Hawaii at Manoa, Honolulu HI 96822, USA.

[4]Geological Museum, University of Copenhagen, Oester Voldgade 5-7, DK-1350, Copenhagen K, Denmark.

The sedimentary sequences of all sites drilled during Leg 166 are strongly influenced by changes in sea level (Eberli, Swart, Malone, et al., 1997). The Neogene section of all recovered cores displays centimeter-to-meter cyclic alterations in the composition and degree of lithification. Sea-level highstands flooded the adjacent platform and resulted in a dramatic increase in platform-derived sediments and organic material (Fig. 2). Lowstands reduced the supply of platform sediments and created periods of nondeposition at the more proximal sites. At the distal sites, lowstands reduced the supply of platform material and organic matter and increased the supply of detrital material (clays) from exposed shelf areas further south. Calci-turbidites from bank tops and slope areas are observed in both highstand and lowstand periods, particularly at the toe of the slope (Site 1007). Turbidites have the effect of mixing sediments, which increases their diagenetic potential by (1) increasing their permeability through sorting, and (2) reoxidizing the turbidite sequence (Cranston and Buckley, 1990). Turbidite sequences in all cores show the highest degree of carbonate recrystallization and the lowest preservation of metastable aragonite.

The nature and magnitude of diagenetic reactions is influenced by the original composition of sediments. Sediments cored along the Bahamas Transect are composed mainly of carbonate (>90 wt%); however, important differences occur with regard to whether the carbonate is derived from neritic or pelagic sources, and in the abundance of organic and siliciclastic components (Fig. 3). These components vary among different depositional sequences and within individual sequences as a function of distance from the platform. Neritic material consists of skeletal fragments composed of metastable aragonite and high-magnesium calcite (HMC) derived from the platform during highstands. Pelagic material mainly consists of foraminifers composed of low-magnesium calcite (LMC). In general, neritic material is more common at the proximal sites, whereas pelagic material and siliciclastics are more common at the distal sites (Sites 1006 and 1007). As might be expected, diagenetic overprinting varies both as a function of distance from the platform margin and as a function of character of each lowstand or highstand deposit. The upper Pliocene–Pleistocene sequences were deposited during a rimmed platform, and have a distinctive mineralogy gradient away from the platform margin. Sediments are characterized by an abundance of aragonite (>70 wt%), with minor amounts of HMC, LMC, and dolomite (Fig. 3). The amount of deposited insoluble clays increases laterally away from the platform and is highest in the on-lapping drift deposits (Fig. 3). In contrast, the Miocene sediments were deposited in a ramp setting and show less lateral variation away from the platform (Eberli, Swart, Malone, et al., 1997).

METHODS

Pore-Fluid Chemistry

The interstitial water chemical data from Sites 1003, 1005, 1006 and 1007 discussed in this paper are mainly based on shipboard mea-

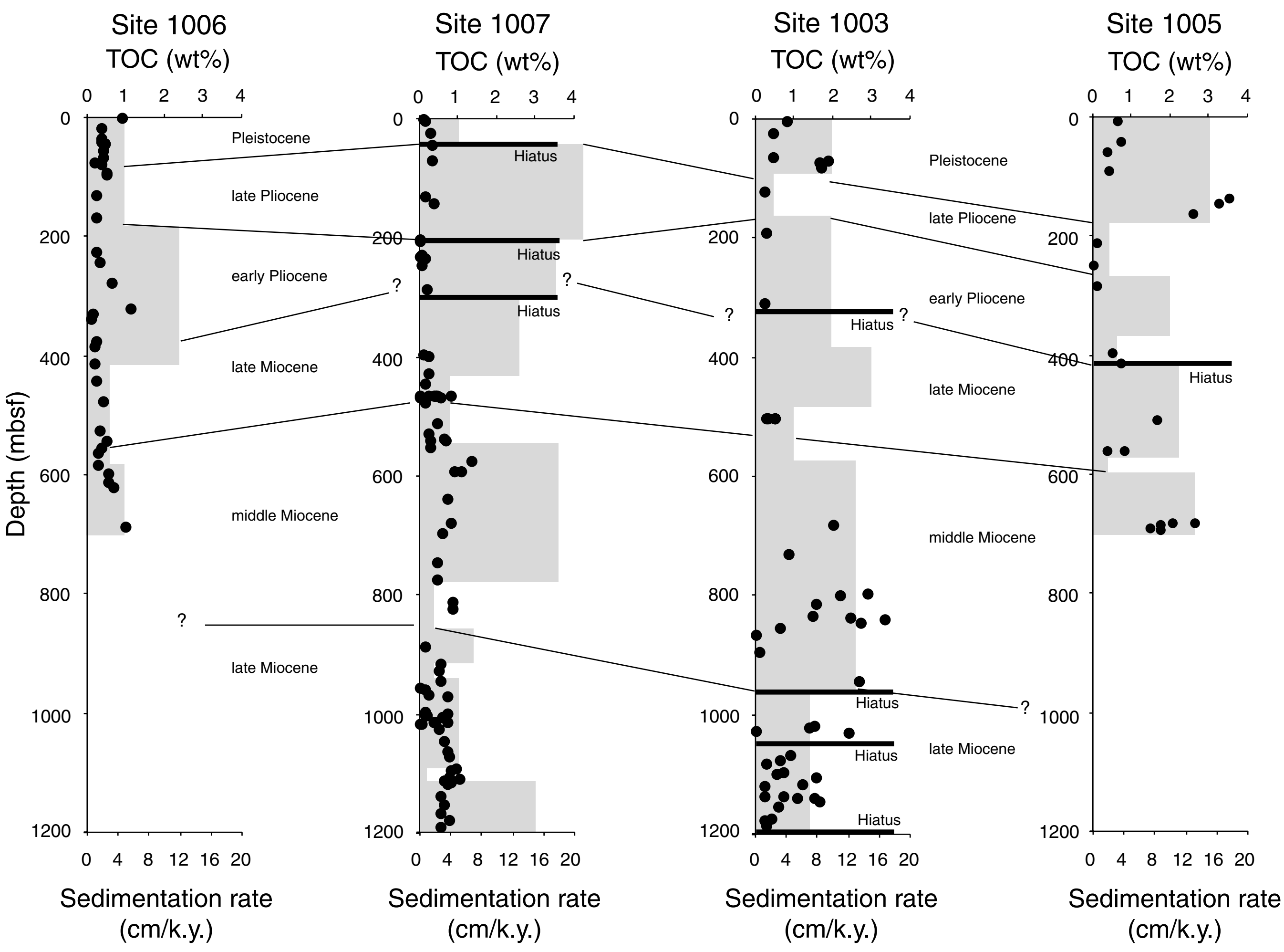

Figure 2. Sedimentation rate (shaded gray areas) and concentration of total organic carbon (TOC; solid black circles) plotted for Sites 1006, 1007, 1003, and 1005. Sedimentation rates and time lines are based on shipboard biostratigraphic data.

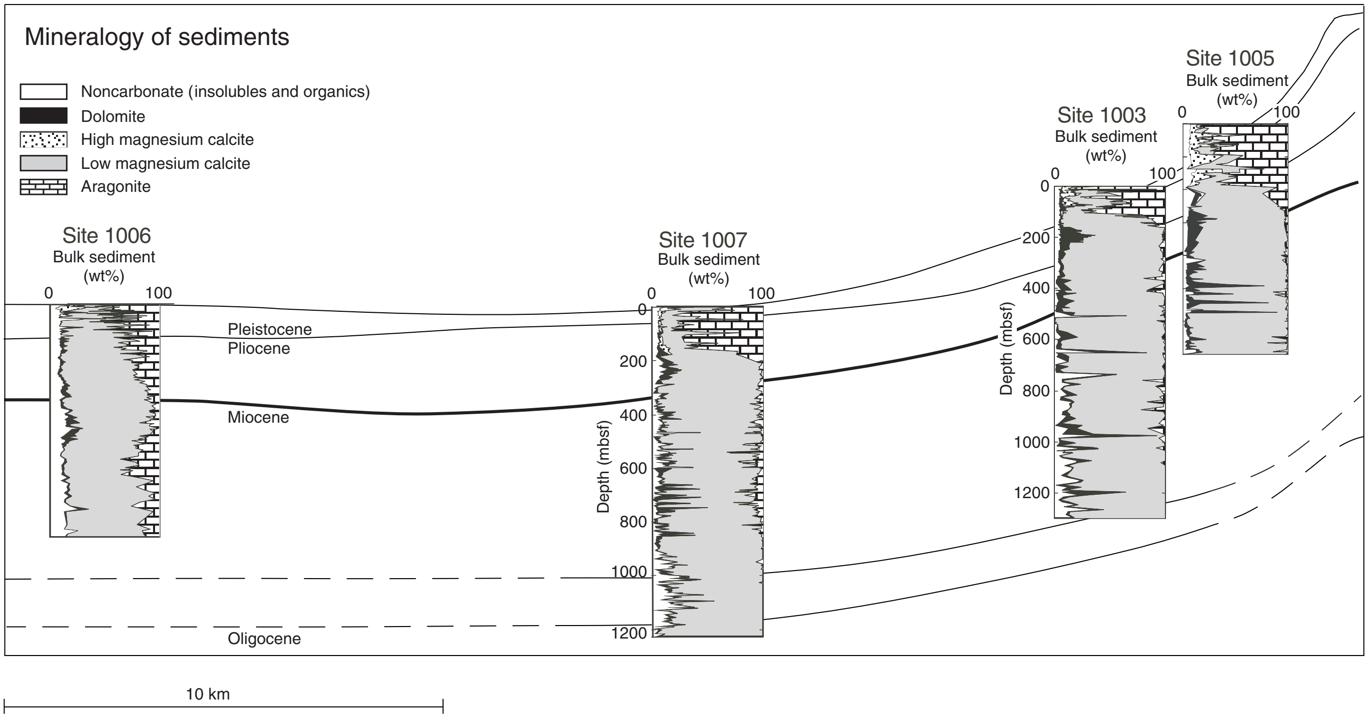

Figure 3. Quantitative X-ray mineralogy and insoluble weight percent of sediments for Sites 1006, 1007, 1003, and 1005 superimposed on an interpreted seismic section.

surements (Eberli, Swart, Malone, et al., 1997). The oxygen stable isotope data and some of the minor and trace element data are from other papers presented in DeCarlo and Kramer (Chap. 9, this volume) and Swart (Chap. 8, this volume). The reader is referred to these references for details on the analytical techniques. Several of the interstitial component shipboard and shore-based analyses are not discussed here, including those for lithium, fluoride, iron, and manganese. A large number of shipboard samples were processed during Leg 166 (generally >40 samples/hole) to allow for the detailed structure in the dissolved constituent profiles to be resolved. A summary of the shipboard pore-fluid results discussed in this paper is presented in Table 1.

Sediment Chemistry

The solid-phase data presented here were obtained from 190 samples collected from Sites 1007 and 1005. Approximately 200 mg of each sample was washed, crushed, dried, and weighed, and then placed in 40 mL of a 20% acetic-acid solution for 2 hr. The acid leachate was filtered through 0.2-µm preweighed filters and analyzed for Li^+, Na^+, Ca^{2+}, Mg^{2+}, Sr^{2+}, Fe^{2+}, Mn^{2+}, and Ba^{2+} on an inductively coupled plasma-mass spectrometer (ICP-MS). Selected samples were analyzed for Ca, Mg, and Sr values using an inductively coupled plasma-optical emission spectroscope (ICP-OES). The concentration of Fe was determined using flame atomic adsorption (AA). All instruments were calibrated using a series of spiked standards in a 20% acetic-acid matrix. The filters containing insoluble residues were dried overnight at 50°C and reweighed to determine the weight percent of insoluble residue. Replicate analyses yielded results within 1 wt% for insoluble residues and within 5% for minor and trace elements.

Carbon Isotope Analysis

Carbon isotope analyses of the DIC were performed on pore-fluid samples which were fixed with $HgCl_2$ and preserved in sealed glass ampules. Samples were injected into an evacuated serum bottle containing 0.5 cm^3 of H_3PO_4. The CO_2 was removed by purging with He, and then analyzed for $\delta^{13}C$ in a continuous flow, stable isotope ratio mass spectrometer (Europa 20–20). The precision using this method was better than 0.1%.

RESULTS

Pore-Fluid Chemistry

The concentrations of the principal pore-fluid constituents for Sites 1003–1007 are presented in Table 1. Depth profiles are shown for the four principal sites of the Leg 166 transect (Sites 1003, 1005, 1006, and 1007) (Fig. 4). A brief description of the principal trends is given below for each of the main constituents.

Chlorides and Alkalides

Contents of dissolved Cl^- and Na^+ have vertical gradients in the shallow Recent–Pleistocene intervals (~20–40 mbsf) at each site. Below this depth, profiles display a sharp increase in concentration that continues to increase down to the base of all holes. The increase is highest at Site 1005 and lowest at Site 1006 (Fig 4). The maximum dissolved Cl^- concentration occurs near the base of Site 1003 (1190 mbsf) and has a value of 1069 mM, roughly two times that of seawater. The concentrations of dissolved Na^+ and K^+ follow that of dissolved Cl^- at all sites except Site 1006.

Constituents Influenced by Organic Carbon Diagenesis

Total alkalinity profiles increase sharply below 20–40 mbsf, reaching broad maxima between 100 and 300 mbsf at all sites. The highest increases in alkalinity content (>60 mM) occur at Sites 1004 and 1005, whereas the smallest increase (7.9 mM) is observed at Site 1006. A second maximum in alkalinity content is reached below 300 mbsf at Sites 1006 and 1007.

Table 1. Summary of interstitial water chemistry, Sites 1003–1007.

Site	Depth (mbsf)	Salinity	Cl (mM)	Na^+ (mM)	K^+ (mM)	Mg^{2+} (mM)	Ca^{2+} (mM)	Sr^{2+} (µM)	Alkalinity (mM)	SO_4^{2-} (mM)	HPO_4^{2-} (µM)	NH_4^+ (µM)	SiO_2 (µM)	Ba^{2+} (µM)	$\delta^{18}O$ (‰)	$\delta^{13}C$ (‰)
1003	BW	36.0	578	502	11.1	56.3	10.8	94		30.1						
1003	1.5	36.0	580	497	11.1	55.9	11.4	97	2.2	29.8	1	113	56		0.75	–1.26
1003	3.0	36.0	577	494	10.7	55.4	10.8	93	2.6	29.7	1	81	26		0.69	–1.92
1003	4.5	36.0	578	498	10.9	55.5	10.9	94	2.7	30.6	1	134	40		0.84	–1.66
1003	6.0	36.0	578	495	11.0	55.6	10.6	96	2.7	29.2	1	141	42		0.74	–0.78
1003	8.5	36.0	576	491	11.0	55.5	10.8	98	2.8	30.4	1	175	51		0.72	–0.95
1003	10.0	36.0	576	489	11.2	55.9	11.0	98	2.9	29.1	1	167	62		0.71	–0.78
1003	11.5	36.0	575	496	10.7	55.4	10.9	99	2.5	30.6	1	115	47		0.87	0.20
1003	15.0	36.0	574	489	10.8	55.5	10.9	121	2.4	30.2	1	91	69		0.64	1.52
1003	24.0	36.0	575	491	11.1	55.8	11.6	140	2.5	30.0	1	100	69		0.67	0.81
1003	28.8	36.0	575	487	11.3	54.9	11.3	119	2.5	29.3	1	117	69			0.87
1003	42.9	36.5	582	492	11.2	55.3	10.7	239	3.2	29.3	1	306	74			2.48
1003	52.4	37.0	595	501	11.6	55.8	11.2	270	5.3	28.4	1	708	112			2.16
1003	61.5	38.5	620	522	11.8	56.4	9.9	409	5.2	26.1	2	1305	184		0.98	2.04
1003	71.4	41.0	655	568	12.9	55.9	9.6	789	17.8	22.6	3	2547	260		1.23	1.32
1003	74.9	42.0	666	564	13.5	54.2	9.5	851	18.4	21.8	5	2774	262			2.60
1003	86.2	43.0	708	585	13.1	51.5	10.3	1005	25.0	18.7	5	3905	316		1.45	2.19
1003	94.8	44.0	721	610	14.2	52.4	10.8	999	26.0	18.0	4	4530	321		1.66	3.82
1003	107.5	46.0	743	616	14.3	50.2	11.6	999	27.8	16.9	3	5620	325		1.67	1.41
1003	118.5	47.0	774	639	15.5	49.6	12.2	1027	25.6	17.1	3	5285	352			1.45
1003	125.1	47.0	778	641	15.4	48.9	12.2	1235	28.3	17.3	3	6814	364		1.62	0.78
1003	145.8	47.5	789	702	15.7	48.0	12.4	1136	26.8	16.2	2	7096	400		1.60	1.53
1003	154.0	47.0	804	661	16.0	47.6	12.8	1284	27.9	16.0	2	7830	420			0.36
1003	160.6	46.0	794	652	15.5	47.5	12.6	1152	27.5	16.2	12	7234	429		1.76	
1003	195.5	49.5	821	676	16.4	48.2	14.6	1182	29.8	15.6	11	7818	483		1.85	
1003	181.5	49.5	816	675	16.1	47.8	13.7	1187	30.4	15.5	10	7812	586		1.86	–0.07
1003	192.7	50.0	820	681	16.4	48.0	14.0	1195	29.2	15.8	7	8038	628		1.94	0.87
1003	199.4	49.0	828	686	16.4	48.4	14.3	1137	27.7	16.2	14	8224	523		1.88	0.03
1003	207.6	49.5	828	684	16.7	48.6	14.3	1095	27.7	16.5	13	8149	515		1.92	0.84
1003	218.7	49.5	823	677	16.3	49.1	14.7	1098	25.7	16.5	2	7663	494		1.99	
1003	283.2	49.0	815	666	15.8	52.7	18.1	742	18.4	23.1	2	6121	494		2.06	0.93
1003	294.3	51.5	854	703	16.4	52.6	20.5	796	20.3	22.2	8	6828	397		2.16	
1003	321.6	52.5	867	713	17.7	53.8	22.5	834	20.8	22.8	14	6438	464		2.29	2.15
1003	332.8	52.0	855	716	17.0	54.7	22.3	800	19.1	24.3	8	6020	452		2.01	1.60
1003	359.6	53.5	883	730	17.6	54.8	23.3	854	17.8	23.0	5	5932	485		2.30	
1003	446.4	57.0	928	778	17.8	53.6	31.4	708		24.2	3	3691	439		2.48	
1003	455.2	57.0	907	757	17.2	55.6	31.5	749	14.2	27.9	3	3507	582		2.40	3.75
1003	466.0	58.0	952	809	17.8	55.5	34.9	742	14.0	28.4	6	3610	728		2.57	2.26
1003	504.5	45.5	744	627	13.8	49.3	25.1	383		24.5	1	1218	766		1.88	2.55
1003	658.6	60.0	982	823	17.1	58.5	43.6	557		35.2		1587	766			
1003	684.9	62.0	995	831	16.7	62.2	45.6	530		38.7		1224	552			
1003	737.2	60.0	974	813	18.2	55.7	41.6	697		32.1		2466	754			
1003	759.7	59.0	964	799	16.8	54.7	41.1	791		33.0		2514	942		2.64	
1003	773.6	61.0	1001	848	18.5	53.8	43.8	788		33.0		2892	1001		2.51	
1003	820.2	62.0	1018	854	18.4	54.8	43.7	771		32.2		3009	997			
1003	910.1	60.0	1023	844	18.6	44.1	30.3	1384	12.5	9.3		3812	992		2.89	2.13
1003	1002.4	58.0	982	820	16.9	33.5	29.0	2946		4.8		10003	936			
1003	1024.1	57.5	1005	847	16.5	27.8	17.1	3654		2.9		13096	808			
1003	1032.2	57.0	974	825	14.6	30.0	17.1	3804		4.3		12263	777			
1003	1083.6	62.0	1069	902	14.5	29.1	19.8	4380					840			
1004	1.5	36.5	560	490	10.3	56.0	11.2	100	2.7	29.8	1	61	41		0.99	–1.23
1004	4.5	36.5	571	496	10.5	56.5	11.4	101	2.7	29.5	1	63	24		0.88	–0.08
1004	6.7	36.5	575	499	10.5	56.2	11.6	96	2.8	30.2	1	108	28		0.99	–0.67
1004	9.7	36.5	576	499	10.3	56.2	11.5	98		29.1	1	152	37		0.91	–0.58
1004	12.7	36.5	575	496	10.2	56.3	11.2	101	3.2	29.7	2	149	49		0.88	–1.14
1004	16.2	36.5	575	492	10.4	56.1	11.1	102	2.6	29.3	1	85	41		0.99	–0.01
1004	19.2	36.5	574					101	2.4	29.8	1	41	24		0.96	0.03
1004	19.2	36.5	562	498	10.5	55.3	10.7	103	2.5	29.3	1	54	24		1.03	0.89
1004	30.2	36.5	575	498	10.3	55.9	11.0	115	2.5	28.9	1	115	20		0.81	1.13
1004	41.2	36.5	571	498	10.6	56.1	11.5	138	3.2	29.2	1	1687	28		0.90	0.07
1004	50.7	37.0	579	504	10.7	54.5	12.2	262	14.4	25.4	4	1617	58		1.08	–0.83
1004	60.2	39.0	615	530	11.6	50.9	9.0	734	37.7	13.1	5	5131	193		1.23	–2.57
1004	74.2	42.0	662	577	12.3	45.4	6.4	1070	64.8	2.6	6	8300	420		1.62	–0.88
1004	83.7	43.0	685	599	12.8	43.0	6.0	1190	70.0	2.2	5	11867	497		1.70	0.56
1004	92.7	44.0	680	605	13.3	43.1	6.7	1365	73.4	1.2	5	13781	507		1.82	0.30
1004	110.4	45.5	711	628	13.7	40.8	6.9	1442	69.4	3.2	9	14912	864		1.72	1.66
1004	130.4	46.0	728	640	14.2	38.8	6.1	1567	65.2	2.3	4	16275	734			
1004	149.8	46.0	734	642	14.5	39.0	6.1	1647	65.2	2.1	4	16478	444		2.14	
1004	185.6	46.5	759	652	15.2	37.7	6.4	2530	68.3	0.3	4	19117	551			
1005	1.5	36.5	583	511	10.5	56.9	11.2	95	2.4	29.9	0	41	33	0	1.06	0.15
1005	4.0	36.5	580	499	10.4	56.7	11.2	100	2.8	29.9	1	93	41	0	1.14	–0.35
1005	6.9	36.5	581	503	10.2	56.4	11.2	101	3.1	30.0	1	152	45	0	1.03	–0.40
1005	9.9	36.5	586	503	10.4	56.7	11.3	95	3.0	29.4	1	149	49	0	1.14	–0.63
1005	13.4	36.5	583	510	10.5	57.1	11.5	102	2.6	29.9	1	91	62	0	1.12	–0.32
1005	23.4	36.5	580	495	10.2	55.8	11.3	122	2.6	29.6	0	66	70	0	0.99	1.11
1005	32.9	36.5	580	503	10.3	56.1	11.2	100	2.6	30.7	0	53	37	0	1.04	1.22
1005	42.4	37.0	586	502	10.6	56.4	11.8	139	5.8	28.4	11	581	54	0	1.11	1.32
1005	50.4	38.0	607	534	10.8	55.8	10.8	380	17.8	21.1	1	1771	87	0	1.26	1.15
1005	57.9	40.0	650	546	11.8	53.1	8.6	633	33.4	11.2	4	3731	125	0	1.53	0.28
1005	68.0	42.0	679	572	12.0	50.0	8.1	809	41.7	5.5	2	4963	168	0	1.73	0.03
1005	68.9	42.0	690	579	12.3	49.3	8.0	910	45.8	2.7	3	5761	189	0	1.81	0.18
1005	74.9	44.0	702	600	12.7	48.7	7.3	1023	46.3	1.4	4	5593	202	0	1.91	0.13
1005	87.5	45.0	739	645	13.7	49.8	7.6	1105		0.5	2	6909	215	1	2.03	0.25
1005	94.1	46.0	758	654	13.9	50.0	8.5	1286	48.4	0.9	2	7091	237	1	2.16	–0.51
1005	122.4	49.5	796	668	14.4	59.0	11.2	1231	38.5	11.2	7	6797	271	1	1.98	–1.18
1005	150.3	46.5	760	645	14.2	46.9	8.9	1006	54.1	4.7	12	11316	784	1	1.67	2.78
1005	164.1	46.5	759	652	14.5	41.3	6.3	932	55.4	2.1	9	14535	856	1	1.81	4.86
1005	178.2	46.0	742	645	14.4	41.1	6.1	1097	60.5	3.1	7	15028	748	1	1.80	4.64

Table 1 (continued).

Site	Depth (mbsf)	Salinity	Cl (mM)	Na^+ (mM)	K^+ (mM)	Mg^{2+} (mM)	Ca^{2+} (mM)	Sr^{2+} (µM)	Alkalinity (mM)	SO_4^{2-} (mM)	HPO_4^{2-} (µM)	NH_4^+ (µM)	SiO_2 (µM)	Ba^{2+} (µM)	$\delta^{18}O$ (‰)	$\delta^{13}C$ (‰)
1005	253.8	46.0	756	664	14.9	34.1	6.0	2710	64.0	0.3	4	17435	555	1	1.94	1.56
1005	263.2	46.5	772	669	15.3	32.6	8.3	2908	61.9	0.4	5	17609	552	1	1.92	0.17
1005	286.0	48.0	771	664	14.8	34.5	9.7	3767	57.1	2.1	4	15869	549		1.94	–1.24
1005	296.0	48.0	790	677	15.0	34.0	6.9	3948	44.3	0.7	5	16362	556		2.02	–0.18
1005	308.0	48.5	793	688	15.5	35.0	9.5	4098	53.3	0.9		16072	531	2	2.01	–1.83
1005	328.0	48.5	795	678	15.2	38.2	10.3	4253	51.3	2.5		14129	511	4		–3.08
1005	360.9	50.0	831	693	15.4	43.1	14.0	3064	40.4	5.3	3	10852	440		2.18	–2.38
1005	388.0	50.0	827	685	15.5	47.9	15.3	1308	23.0	12.1	2	7756	379	0	2.12	
1005	405.2	50.0	830	678	16.3	49.0	15.8	930		15.0		7016	317			
1005	416.0	52.0	846	693	16.4	53.8	18.3	806		20.5		5943	329			
1005	425.5	52.0	826	695	16.2	54.3	19.1	631	10.4	21.8		5943	322	0		
1005	433.0	52.0	823	676	15.4	56.5	22.6	707		23.7	4	4537	646			
1005	460.7	52.0	850	716	16.6	59.5	24.3	643	13.3	29.1	4	3279	340	0		
1005	490.1	54.0	878	749	17.3	59.5	26.7	626	9.1	30.3		2428	335	0		
1005	528.3	56.0	891	751	16.0	60.9	29.8	592	13.9	32.5		2502	396	0	2.35	
1005	553.3	50.0	846	685	14.7	51.8	29.0	637		26.8		2206	467			
1005	565.4	56.0	925	758	14.8	52.8	30.7	708	10.1	23.6	3	3908	575	0	2.26	
1005	573.2	56.0	922	756	16.3	52.6	32.3	700		24.2		3464	533			
1005	601.0	56.0	929	777	15.3	51.9	33.7	797	7.8	23.5		3501	578	0		
1005	637.0	57.0	944	782	17.0	51.9	34.1		8.2	25.7	2	3760	357	0		
1005	682.5	57.0	962	799	15.9	46.4	32.4		9.7	16.9		3686	713	1		
1006	2.9	35.0	563	481	10.7	53.7	9.4	154	3.8	27.1	0	127	168	0	0.15	
1006	5.8	35.0	564	482	10.9	53.9	9.6	138	3.1	27.9	0	116	100	0	0.12	
1006	10.0	35.0	560	481	10.2	54.5	9.7	174	2.9	28.4	0	84	60	0	0.11	
1006	14.5	35.0	563	482	10.9	54.3	9.3	180	2.8	27.5	0	88	92	0	0.08	
1006	19.5	35.5	564	482	11.1	54.5	9.5	208	2.9	28.0	0	127	117	0	0.22	
1006	24.0	35.0	566	485	11.5	54.4	9.4	222	3.2	29.0	0	24	119	0	0.15	
1006	29.0	35.5	569	489	11.0	54.1	9.5	455	3.9	27.4	0	222	134	0	0.22	
1006	38.5	36.0	577	499	10.1	51.0	9.2	674	5.5	23.9	0	546	172	0	0.60	
1006	48.0	36.0	589	518	10.8	48.1	8.7	840	6.1	20.9	0	942	189	0	0.57	
1006	57.5	36.0	595	525	10.7	45.0	8.5	992	7.3	17.7	0	1158	193	0	0.70	
1006	67.0	36.0	600	530	10.1	41.6	7.9	1209	7.7	15.4	3	1806	193	2		
1006	76.5	36.0	606	530	10.4	39.1	7.7	1335	7.2	12.7	1	1626	197	1	0.61	
1006	86.0	36.0	616	547	10.3	36.9	7.7	1498	7.8	10.6	2	2058	214	1	0.63	
1006	95.5	36.0	618	542	10.3	35.0	7.3	1670	7.9	9.1	1	2346	231	1	0.46	
1006	105.0	36.0	626	560	9.8	34.0	7.8	1756	7.9	8.2	1	3066	254	1	0.56	
1006	114.5	36.5	630	550	10.4	32.7	9.2	1818	7.2	6.8	0	2652	278	1	0.45	
1006	124.0	37.0	640	556	9.8	32.1	7.6	1958	7.5	6.3	0	2292	273	1	0.39	
1006	133.5	37.0	641	568	10.2	31.0	7.6	2108	6.9	5.7	0	2760	275	1		
1006	143.0	37.0	644	577	9.9	30.8	7.9	2361	7.5	4.1	1	2850	256	1	0.27	
1006	152.5	37.5	653	577	9.7	29.6	8.0	2976	6.2	3.5	1	3192	231	1	0.31	
1006	162.0	37.5	661	575	9.9	28.7	7.9	3138	6.9	3.0	1	2922	218	1	0.31	
1006	171.5	38.0	666	580	9.5	28.1	8.0	3336	6.7	2.2	1	3354	208	2	0.25	
1006	181.0	38.0	668	583	9.5	27.9	8.3	3488	6.7	1.8	1	2958	218	3	0.24	
1006	190.5	38.0	672	595	9.7	27.3	8.5	3720	6.4	1.2	1	3480	231	4	0.32	
1006	200.0	38.5	676	593	9.0	26.8	8.5	3989	6.4	0.7	0	3408	248	10	0.26	
1006	209.5	38.5	676	605	8.9	26.4	8.6	3872	6.2	0.6	0	3570	256		0.25	
1006	219.0	39.0	686	602	9.3	26.3	9.1	4159	5.9	0.2	0	3534	291	30	0.25	
1006	228.5	39.0	693	604	9.1	26.1	9.1	4250	5.9	0.0	0	3768	318		0.28	
1006	238.0	40.0	696	614	9.2	25.6	9.2	4435	5.5	0.0	0	3876	374	35	0.23	
1006	247.5	40.0	699	602	8.4	25.7	9.9	4505	5.1	0.0	0	3570	469		0.23	
1006	257.0	40.0	702	588	8.6	25.6	10.6	4680	5.1	0.0	0	3984	503	39	0.26	
1006	266.5	40.0	706	591	9.1	25.5	11.1	4565	5.1	0.0	0	4056	408		0.25	
1006	276.0	40.5	712	602	9.0	25.8	11.4	4825	4.8	0.0	0	3408	389	43	0.25	
1006	281.8	40.5	715	598	8.5	28.3	11.7	4935	4.7	1.8	1	4218	374			
1006	287.6	40.5						4690	4.7	1.9	0		365	44		
1006	296.8	40.5	708	589	8.0	28.3	11.8	4800	4.6	0.0	0	4056	363			
1006	306.0	41.0	726	622	8.1	26.3	12.6	5075	4.7	0.0	0	4290	498	56		
1006	315.3	42.0	731	636	8.7	26.5	12.9	5355	4.9	0.0	0	4344	644	58		
1006	342.7	42.0	743	619	8.3	27.4	15.4	5620	5.3	0.0	0	4470	522	113		
1006	370.2	43.0	759	627	7.9	27.5	14.2	6103	5.8	0.0	0	4758	449	92		
1006	397.6	44.0	766	636	7.7	28.4	14.7	6150	6.1	0.0	0	4938	689	117		
1006	425.7	44.5	783	644	8.0	29.5	14.6	6353	6.5	0.0	0	4704	642	155		
1006	453.0	46.0	795	652	7.6	31.1	14.6	7005	7.5	0.0	0	5460	425	206		
1006	481.0	46.0	803	703	8.0	34.2	15.4	6550	7.5	0.0	0	5370	387	228		
1006	512.8	46.5	815	671	7.6	33.1	14.4	6445	7.0	0.0	0	4920	373	186		
1006	537.2	47.0	820	697	7.4	33.8	14.9	6600	6.5	0.0	0	5568	376	160		
1006	566.1	48.0	827	676	6.9	34.6	16.0	6405	7.0	0.0	0	5100	434	59		
1006	595.0	48.0	843	694	7.1	35.3	16.5	6305	6.3	0.0	1	5208	662	154		
1006	626.9	49.0	859	720	7.0	35.4	18.2	6055	6.2	0.0	1	5640	807	214		
1006	666.9	50.0	865	710	6.6	36.5	19.1	5380	6.7	0.0	1	4632	835	43		
1006	691.3	48.5	839	682	6.9	35.7	18.2	4560	5.8	1.9	0	5352	853	9		
1006	710.6	50.0	866	707	6.6	37.1	19.3	5310	5.8	1.1	0	5586	699	49		
1007	5.9	35.5	562	475	10.3	53.6	10.9	129	2.9	28.2	1	47	50	3	0.44	
1007	9.0	36.0	564	472	10.1	53.7	10.7	130	2.8	28.4	1	44	44	1	0.35	
1007	12.4	35.0	561	474	10.5	52.6	10.6	128	2.5	28.4	2	50	56	1	0.39	
1007	15.4	35.5	562	479	10.4	53.3	11.0	145	2.7	29.2	1	57	58	2	0.39	
1007	21.9	35.5	564	481	10.4	53.8	10.5	190	3.0	28.0	1	83	58	0	0.52	
1007	24.9	35.5	565	485	10.1	53.2	11.0	240	3.5	28.3	0	134	75		0.48	
1007	35.9	36.0	585	496	11.6	53.7	11.1	469	7.2	27.3	2	920	125	1	0.60	
1007	47.4	39.5	631	544	11.6	55.6	11.0	794	14.2	24.5	4	1718	197	1	1.07	
1007	53.9	40.5	649	553	11.7	56.1	10.5	863	16.2	23.0	5	2033	228	1	1.20	
1007	64.9	41.0	679	576	11.6	56.8	10.2	860	19.9	21.4	4	2369	242	1	1.28	
1007	72.9	42.5	689	585	11.9	57.1	10.0	968	20.5	20.9	16	2390	286	1	1.32	
1007	82.4	43.5	706	607	12.5	57.3	9.8	937	22.1	19.6	5	2684	294	1	1.34	
1007	87.6	44.0	729	600	12.5	57.0	9.7	1078	22.3	19.9	7	2327	294	1	1.33	
1007	96.1	44.5	727	619	13.5	56.9	9.3	1050	20.0	19.8	4	2684	300	1	1.38	
1007	136.9	48.5	782	676	13.6	60.0	11.4	1071	24.5	22.1	4	2852	294	0	1.46	

Table 1 (continued).

Site	Depth (mbsf)	Salinity	Cl (mM)	Na^+ (mM)	K^+ (mM)	Mg^{2+} (mM)	Ca^{2+} (mM)	Sr^{2+} (µM)	Alkalinity (mM)	SO_4^{2-} (mM)	HPO_4^{2-} (µM)	NH_4^+ (µM)	SiO_2 (µM)	Ba^{2+} (µM)	$\delta^{18}O$ (‰)	$\delta^{13}C$ (‰)
1007	142.9	49.0	796	676	14.4	60.9	10.9	999	21.3	22.4	4	3335	278	0	1.56	
1007	153.3	49.5	796	674	13.6	61.3	12.1	1004	23.6	22.5	3	2999	286	0	1.47	
1007	158.3	49.5	803	689	14.3	63.0	12.0	898	22.9	23.1	4	3188	297		1.58	
1007	209.0	53.5	858	729	16.2	62.5	16.8	824	16.5	26.1	2	3167	339	0	1.86	
1007	219.8	54.0	870	744	16.2	62.3	18.2	765	16.4	26.9	2	2894	350		1.98	
1007	228.9	54.0	871	743	16.1	61.8	18.8	789	14.8	27.0	2	3146	317	0	1.96	
1007	238.0	54.0	885	742	16.7	61.5	19.9	806	14.3	27.4	2	3167	317	0	2.09	
1007	247.2	55.0	888	748	16.1	62.0	20.5	747	12.5	28.2	1	2747	286	0	2.11	
1007	253.5	54.5	882	752	15.9	61.0	21.5	755	14.6	28.0	1	2432	300		2.11	
1007	259.8	55.0	894	754	15.7	60.6	21.7	721	13.0	28.4	2	3020	312	0	2.17	
1007	270.6	55.5	897	742	15.8	60.0	23.1	754	12.7	27.9	2	2873	343	1	2.07	
1007	287.4	55.0	905	738	15.8	59.4	24.0	723	11.7	28.4		2159	318		2.27	
1007	341.1	55.0	901	755	16.0	59.2	26.3	708	13.9	29.4	2	2285	242	0	2.36	
1007	351.4	55.0	897	745	16.0	59.3	26.4	704	11.1	28.7	2	2495	241	0	2.26	
1007	409.9	56.5	917	771	16.4	58.5	24.1	869	13.5	25.1	2	2663	247	0	2.49	
1007	428.1	56.0	923	759	15.7	57.1	23.1	917	11.3	24.8	1	3083	245		2.38	
1007	440.4	56.5	934	773	15.9	56.7	22.5	941	10.3	23.3	1	3272	235	0	2.48	
1007	463.3	56.0	932	769	16.5	54.8	22.9	935	9.8	22.2	1	3524	403	0		
1007	479.1	56.0	931	788	15.8	54.6	25.5	843	8.4	22.8	2	4049	401	1	2.45	
1007	497.0	54.5	912	760	16.6	44.8	20.4	1347	10.5	14.8	3	5435	769	1		
1007	530.4	53.5	926	773	15.7	35.9	14.8	2960	10.2	7.1	1	6170	674	2		
1007	549.4	53.0	934	780	15.4	34.2	13.8	3401	8.2	6.4	2	7598	630	3	2.42	
1007	565.3	53.0	961	779	16.5	33.6	14.8	3237	10.8	5.7	2	7031	779	4		
1007	597.5	54.0	925	772	15.3	33.8	15.4	3462	14.0	5.3	2	6842	895	10	2.40	
1007	620.8	54.0	925	776	16.3	29.0	13.4	4030	19.1	2.1	6	8228	786	12	2.42	
1007	648.3	52.0	899	754	15.8	27.9	12.1	3504	14.7	2.2	2	7472	775	12	2.19	
1007	682.2	52.0	914	772	16.5	26.3	11.5	3443	15.4	1.5	2	8984	698			
1007	708.3	52.5	920	785	16.4	27.0	11.5	3725	11.2	1.2	2	10433	705	20	2.38	
1007	726.7	52.5	930	774	18.5	27.6	11.8	3095	9.6	2.2	2	10139	599	31		
1007	745.7	54.0	945	803	17.6	28.7	14.1	3802	10.9	1.3	3	9068	725	38		
1007	766.3	54.0	951	811	15.8	29.9	14.7	3960	14.4	1.3	0	10034	723	16		
1007	794.4	54.0	911	760	16.5	31.7	14.4	3920	18.1	3.2	0	8879	731			
1007	814.8	54.0	943	793	17.3	31.4	15.0	4465		3.5		6632	771	25		
1007	842.1	54.5	955	820	17.0	31.4	15.0	4095	15.3	1.7		11131	729	27		
1007	870.5	55.5	968	801	15.4	30.3	14.9	4330	18.2	0.8		12015		11		
1007	890.1	55.0	957	786	15.4	30.3	14.2	3830	16.7	2.5		10655		68		
1007	929.0	56.5	1001	827	14.3	27.6	15.5	4780	11.5	0.7	0	12491				
1007	986.4	55.5	971	820	12.9	27.6	15.1	4300		1.8		10281				
1007	1014.4		809	688	10.0	22.3	14.2	3740		3.5		6592				

Notes: BW = surface bank water; blank cells = not measured.

Ammonium (NH_4^+) profiles are similar to alkalinity profiles in the upper 200 mbsf, with a broad maximum between 4 and 15 mM obtained 20–50 m below the alkalinity peak. The occurrence of the NH_4^+ peak at greater depths than the sulfate peak is probably caused by differences in microbial end products within the sulfate reduction zone and lower methanogenic zone. Ammonium content either continues to increase to the base of the hole (Sites 1006 and 1007), decreases (Site 1005), or displays a second maximum near the base of the hole (Site 1003). The content of dissolved phosphate was very low at all sites (<6 µM) and is limited by a strong interaction with carbonate (Kitano et al., 1978).

Sulfate (SO_4^{2-}) profiles decrease sharply below 30 mbsf and reach a broad minimum between 80 and 200 mbsf at all sites. The sharpest decrease occurs at Site 1005, where SO_4^{2-} becomes undetectable (<2 mM) by a depth of 80 mbsf. At Site 1003, the minimum SO_4^{2-} concentration is 15.5 mM at a depth of 181 mbsf. Interestingly, at both Sites 1003 and 1005 the concentration of SO_4^{2-} increases further downhole in excess of bottom-water concentrations (30 mM). At Site 1003, SO_4^{2-} concentrations as high as 38.7 mM occur at a depth of 687 mbsf. (Table 1). In contrast, Sites 1006 and 1007 display a more typical SO_4^{2-} profile of decreasing concentration with depth in the upper 200 mbsf (base of sulfate reduction zone), and low to zero concentration down to the base of the hole.

Alkaline Earth Elements

Calcium (Ca^{2+}) and magnesium (Mg^{2+}) profiles show significant differences between sites and considerable structure within each site (Fig. 4). As with the other elements, the profiles are near vertical in the upper 20–30 m of each site, with concentrations similar to bottom-water values. Large changes occur below the base of this zone. Calcium concentrations range between 6 and 34 mM, with significant decreases from seawater concentrations within shallow (upper 200 mbsf) zones of active sulfate reduction, and significant increases further downhole. Magnesium concentrations range between 25 and 63 mM, and generally decrease with depth at all sites. Strontium (Sr^{2+}) concentrations increase to very high values below 30 mbsf at all sites. The highest concentration (~7 mM) was recorded at a depth of 453 mbsf at Site 1006. At Sites 1003, 1005, and 1007, Sr^{2+} concentrations decrease further downhole in an inverse relationship with SO_4^{2-}. Dissolved barium (Ba^{2+}) ranges between 0.1 and 227 µM, with higher concentrations measured at the more distal sites. Barium profiles similarly show an inverse relationship with respect to SO_4^{2-}.

Oxygen and Carbon Stable Isotopes

The oxygen stable isotopic composition ($\delta^{18}O$) of interstitial waters ranged from +0.05‰ to +0.08‰ in the upper 30 mbsf at all sites, becoming heavier further downhole at all sites except Site 1006. The highest $\delta^{18}O$ values (+2.8‰) occurred at Site 1003 at a depth of 910 mbsf. The carbon stable isotopic composition ($\delta^{13}C$) ranged from –2.57‰ to +4.86‰, with a mean value of +0.17‰.

Minor and Trace Element Composition of Acid Soluble Solid Samples

Minor and trace element composition of the acid soluble sediment samples at Sites 1007 and 1005 are shown in Table 2. Also included are sediment porosity data determined by pycnometer on the same samples (F. Anselmetti and J. Kenter, unpubl. data). The insoluble content at Site 1007 ranges between 0.5% and 36%, with significant cyclic variation within the Miocene sequences. At Site 1005, insoluble content ranges between 1.5% and 10.5%. Strontium concentrations vary from 500 to 12,000 ppm. Iron concentrations range from 50 to 1800 ppm, with the highest values associated with higher insoluble fractions. Manganese concentrations vary from 0 to 220 ppm,

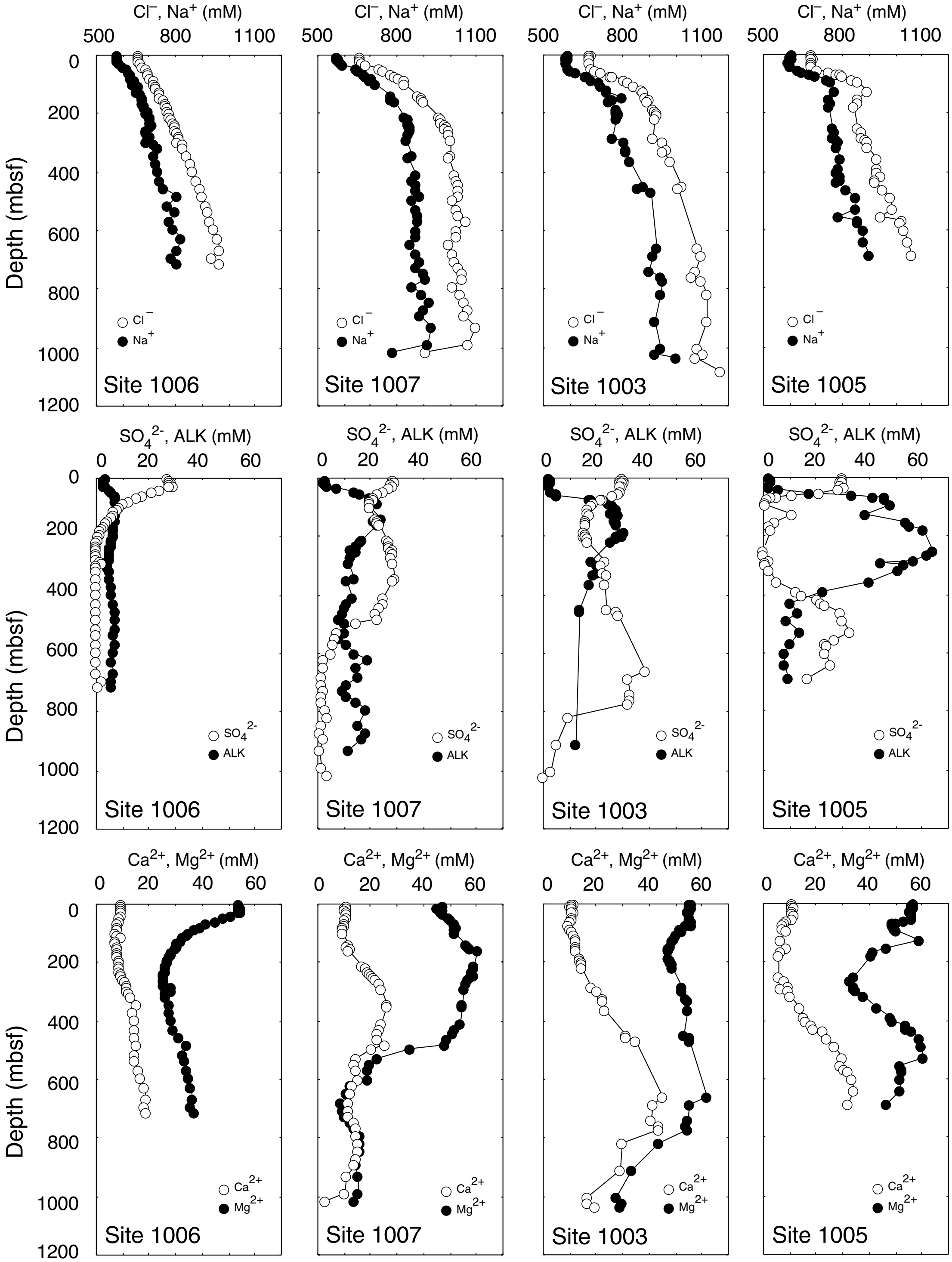

Figure 4. Depth profiles of selected interstitial water constituents for Sites 1006, 1007, 1003, and 1005. ALK = alkalinity.

displaying clear cyclic intervals downhole. Barium concentrations vary from 4 to 274 ppm and show distinct patterns downhole that are probably related to the abundance of acid-soluble barite in the sediments.

DISCUSSION

In this section, discussion is limited to those aspects of the pore-fluid data that are relevant to the fluid flow objectives and that highlight the significant diagenetic results of the Bahamas Transect. The discussion has been divided into four parts that cover the most intriguing hydrogeochemical features of the Transect. These are (1) the shallow pore-fluid gradient shifts, (2) the Na^+ and Cl^- profiles, (3) the carbonate diagenesis, and (4) the organic matter diagenesis.

Shallow Pore-Fluid Gradient Shifts

Pore-fluid profiles display a dramatic shift in the upper 100 mbsf at all sites. In the upper 20–40 m, profiles of typically conservative

Table 2. Elemental composition of sediments, Sites 1005 and 1007.

Site	Depth (mbsf)	Insolubles (wt%)	Porosity (%)	Mg (%)	Fe (ppm)	Na (ppm)	Mn (ppm)	Sr (ppm)	Ba (ppm)	Li (ppm)
1005	128.8	2.9	21.0	1.8	128	3346	25	2420	7	
1005	138.1	3.0	30.0	1.2	79	4570	19	3310	6	
1005	138.3	2.8	31.0	1.7	40	3970	14	2850	5	
1005	151.2	4.0	34.0	0.9	100	5163	27	3470	7	
1005	454.0	2.9	23.0	4.9	122	3095	12	2030	6	
1005	387.9	3.0	38.0	0.9	88	4083	11	1640	2	
1005	425.4	2.9	29.0	1.5	89	2898	10	1470	3	
1005	434.9	1.5	35.0	1.4	103	3095	11	1370	10	
1005	452.9	4.7	20.0	7.0	106	2406	13	2080	7	
1005	470.1	3.1	36.0	0.8	93	3250	12	2100	3	
1005	472.7	2.6	8.0	1.0	60	1234	10	1990	3	
1005	509.0	3.1	25.0	1.2	81	2933	12	2170	3	
1005	553.6	3.9	34.0	0.7	146	3864	16	2520	4	
1005	564.1	9.0	20.0	0.5	152	3168	53	3230	6	
1005	566.9	3.2	31.0	0.7	88	3213	13	2650	4	
1005	581.0	3.4	19.0	0.4	188	1962	18	2970	5	
1005	591.4	8.8	36.0	0.9	323	4709	34	2600	6	
1005	599.9	1.5	13.0	0.6	88	1553	14	3410	6	
1005	600.8	3.6	6.0	0.5	94	1119	16	3910	5	
1005	602.5	10.5	45.0	0.4	288	9204	19	3560	6	
1005	618.9	6.6	38.0	1.8	407	6416	47	2020	5	
1007	95.3	1.6	46.6	1.5	443	4530	65	3200	7	9
1007	132.6	3.6		0.7	137	7734	29	5687	12	
1007	142.4	3.1		0.8	47	3137	21	3015	9	
1007	145.2	3.0		0.8	54	8301	4	8591	7	
1007	155.1	6.4	16.1	1.4	257	2227	32	3460	11	9
1007	166.1	0.8	40.0	1.5	97	4514	27	3160	6	13
1007	166.5	3.9	50.2	1.3	275	6698	46	3222	6	
1007	203.3	9.4		0.9	568	8919	113	1678	10	
1007	206.0	8.8		0.8	805	10772	140	1716	6	
1007	214.8	8.3		1.3	476	8627	92	1505	4	
1007	221.4	7.3		0.9	596	9445	90	1446	21	
1007	221.6	8.5		0.8	194	8401	94	1310	3	
1007	227.6	8.3		1.0	380	9462	97	1460	4	
1007	229.6	19.6		0.9	488	10818	91	1554	3	
1007	232.9	10.9		1.1	499	9045	94	1577	5	
1007	235.6	12.7	50.6	1.0	457	7572	55	7410	131	
1007	241.8	4.9	51.0	1.4	592	7391	76	1640	4	19
1007	250.1	16.6	44.8	0.8	899	8546	64	1618	7	
1007	254.4	5.2		0.9	523	7333	28	1176	4	
1007	258.5	5.8	51.1	1.0	406	5750	49	1100	5	
1007	268.1	6.0	39.8	0.9	155	5610	29	3743	36	
1007	272.4	4.8		0.6	178	4508	24	1157	2	
1007	277.2	4.8		0.6	312	6066	30	1174	3	
1007	288.1	6.7		0.8	444	8752	90	1708	4	
1007	295.4	5.5		0.4	245	5621	37	1254	4	
1007	332.6	6.5		0.6	1117	7888	42	1616	4	
1007	342.8	4.0	42.8	0.5	185	5931	26	1737	2	
1007	341.7	6.9	45.5	0.6	405	6098	32	1803	4	
1007	351.2	2.5	36.9	0.8	76	5522	24	2080	3	12
1007	351.3	4.6	38.0	0.6	170	5594	22	2069	2	
1007	360.2	3.2	10.3	0.6	58	1603	12	2436	3	
1007	368.7	3.5	15.4	0.5	91	1663	23	1882	3	
1007	302.8	0.4	43.2	0.8	81	3294	18	1660	3	11
1007	322.0	6.8		0.5	178	7735	53	1663	2	
1007	323.3	5.7	48.6	0.6	597	5758	54	1640	4	15
1007	330.8	4.2		0.5	79	4041	32	1673	3	
1007	342.5	8.9	43.6	0.5	527	7328	52	2689	7	
1007	353.4	4.3		0.4	118	2465	23	2000	3	
1007	361.5	3.4	31.1	0.5	42	2871	15	2072	4	
1007	351.9	4.7	39.8	0.5	93	4890	21	1915	3	
1007	362.6	1.9	14.8	0.8	161	1546	23	1980	3	12
1007	372.8	4.9		0.7	187	2640	33	4178	118	
1007	389.1	10.5	42.8	0.7	206	7658	52	3302	7	
1007	389.7	6.6		0.9	356	4650	37	6505	91	
1007	399.0	7.0	37.6	0.6	305	4671	46	2206	6	
1007	409.3	13.3	41.1	1.6	619	6672	65	14205	27	
1007	410.8	5.4	23.2	0.5	210	2685	33	2375	6	
1007	419.0	4.6		0.5	221	2547	37	2642	8	
1007	428.6	12.5	44.0	0.4	643	7913	60	10816	39	
1007	427.1	4.7		0.4	218	2348	43	2580	6	
1007	408.7	10.3		0.7	594	7819	68	2955	8	
1007	389.6	6.6		0.8	167	4519	39	4619	42	
1007	382.6	4.8		0.6	166	1946	36	2338	5	
1007	439.3	11.6	43.5	0.3	327	9309	48	4209	8	
1007	438.6	6.7		0.4	135	4510	40	2176	7	
1007	448.6	9.2		0.5	179	8224	73	3404	9	
1007	448.0	5.9		0.4	122	1930	47	2899	9	
1007	460.5	7.8	28.7	0.3	512	3595	59	2935	18	
1007	471.9	3.1		0.5	58	936	38	1851	11	
1007	468.0	4.4	12.8	1.8	25	1813	81	3770	13	10
1007	468.1	4.8	13.6	1.7	27	1671	91	3920	13	11
1007	468.1	5.1	13.5	1.8	37	1792	77	3030	9	12
1007	468.2	8.4	20.5	2.4	50	2428	55	2250	7	14
1007	468.3	17.5	32.5	5.8	86	5774	63	2850	8	18
1007	468.4	26.8	34.8	8.2	131	8243	65	3070	10	24
1007	468.5	34.0	40.3	11.8	178	11819	62	3670	13	72
1007	468.7	19.0	39.9	6.4	121	6406	74	2820	11	187

Table 2 (continued).

Site	Depth (mbsf)	Insolubles (wt%)	Porosity (%)	Mg (%)	Fe (ppm)	Na (ppm)	Mn (ppm)	Sr (ppm)	Ba (ppm)	Li (ppm)
1007	468.8	13.6	39.3	6.7	114	6665	83	3860	24	0
1007	468.9	4.0	13.9	1.8	48	1770	113	3260	10	13
1007	469.0	3.7	11.5	1.3	29	1338	74	3590	13	16
1007	469.1	3.2	11.6	1.4	0	1371	71	3420	14	16
1007	469.3	2.7	10.2	1.4	48	1364	68	3970	16	11
1007	475.7	10.2	37.6	0.5	432	4895	65	2716	11	
1007	479.6	5.4	31.9	0.4	147	3043	35	2935	18	
1007	481.6	3.0		0.7	53	637	18	3126	21	
1007	485.8	8.6		0.8	298	7353	83	2701	12	
1007	495.8	13.8		0.5	304	6571	161	1907	12	
1007	497.2	5.7		0.3	160	1943	46	3550	16	
1007	499.5	12.8		0.6	508	8239	56	3394	11	
1007	505.2	11.6	48.1	0.4	370	11078	25	5931	10	
1007	507.2	9.6		0.5	158	8770	24	4868	15	
1007	515.0	16.0		0.5	314	8340	56	3411	19	
1007	516.2	6.7	20.3	0.3	451	3289	52	3563	12	
1007	521.4	7.5		0.3	250	3628	31	3489	16	
1007	535.8	7.6		0.3	292	3001	26	4401	18	
1007	526.1	17.7	41.0	1.1	451	9379	58	4311	17	
1007	530.7	6.3	39.2	0.5	179	5903	24	2464	19	
1007	539.1	16.2	44.3	0.3	383	9948	46	5339	17	
1007	536.0	7.7	23.4	0.3	277	3734	34	3951	25	
1007	557.0	5.3		0.3	153	2464	26	3731	31	
1007	575.3	7.7		0.5	249	3507	37	4109	30	
1007	542.6	9.1	26.4	0.4	283	5357	34	3890	22	
1007	564.1	4.2		0.6	134	2887	16	3838	37	
1007	572.7	16.6		0.8	384	10361	38	4914	26	
1007	601.4	4.2	17.7	1.0	147	1911	17	2733	27	
1007	621.1	5.9		3.7	283	3451	18	2771	28	
1007	641.3	4.3		0.7	109	2413	13	3142	30	16
1007	658.8	1.5	18.2	3.5	344	3180	43	4110	45	22
1007	660.7	3.7		0.7	57	2966	11	3139	21	
1007	667.9	4.8		0.8	137	2355	12	3098	22	25
1007	678.1	1.9		1.1	643	7894	50	3850	30	17
1007	698.9	5.0		2.4	840	3690	60	4280	36	23
1007	715.6	3.0		0.7	21	2054	6	3869	20	
1007	756.3	5.2		0.6	163	1949	17	5526	248	
1007	690.6	3.7	21.0	1.1	104	2739	8	2901	19	
1007	696.9	3.9	44.8	0.9	93	1877	16	4230	35	19
1007	709.7	0.5	11.5	1.1	353	4317	32	4210	30	25
1007	718.5	3.1	14.3	1.4	29	2537	5	3549	20	20
1007	719.1	3.7		6.3	28	842	3	2047	16	20
1007	745.6	3.7		0.6	94	2902	38	4286	54	30
1007	745.9	20.9	10.7	8.4	404	3097	19	4170	32	38
1007	774.3	7.1	44.5	0.4	249	7042	11	8540	36	24
1007	778.3	4.6	16.3	0.4	168	2056	29	2859	49	20
1007	795.5	12.6	39.6	1.0	64	2196	12	4480	30	14
1007	822.7	10.9	39.9	1.3	290	7876	31	3174	85	22
1007	823.9	1.4	15.6	0.5	451	7133	36	6450	81	21
1007	834.3	1.4	5.2	2.4	137	2285	26	5700	78	17
1007	844.4	4.1	19.0	1.0	145	2109	16	4170	117	19
1007	842.1	6.9	45.3	0.5	414	8023	34	5410	75	19
1007	861.8	10.9	19.5	0.8	233	3628	29	2671	88	17
1007	851.0	14.1	24.0	3.8	351	3702	36	3481	135	21
1007	879.1	5.0		0.5	381	7854	24	7860	92	20
1007	890.4	10.5	36.2	1.5	141	2013	25	3950	110	17
1007	901.2	11.0		0.3	180	3928	41	2298	59	16
1007	900.7	10.8	40.1	0.9	95	1528	19	3850	136	25
1007	908.2	1.3		0.4	465	7061	28	5950	138	55
1007	919.9	16.1	39.1	1.1	432	7767	43	1706	72	20
1007	918.1	13.3	28.3	0.5	515	6068	76	2844	104	
1007	921.1	11.7	41.8	1.0	870	10154	64	2273	77	
1007	927.7	18.1	44.7	0.4	248	3197	63	3043	42	18
1007	927.5	7.2	23.3	0.6	67	1265	18	3593	85	
1007	938.2	3.1	9.7	0.6	27	1444	26	3901	104	21
1007	938.4	4.2	15.2	0.6	728	5545	72	2490	97	24
1007	962.1	7.0	21.4	0.4	223	3752	59	2693	35	13
1007	963.3	18.0	36.5	0.4	607	8496	66	2178	62	17
1007	971.3	19.2	41.1	0.6	392	9998	71	2322	57	11
1007	976.7	3.3	17.0	0.6	178	2405	13	3193	39	
1007	986.4	8.0		1.0	190	2455	41	3223	65	20
1007	995.8	12.0	35.5	1.0	835	7188	66	1997	32	
1007	999.6	14.1		0.8	434	6016	104	2147	27	
1007	1025.0	2.6		1.0	72	584	19	2918	38	
1007	1015.0	22.1	10.0	1.6	682	3009	137	2226	32	
1007	1019.4	14.9	21.4	1.0	442	4143	59	2592	28	17
1007	1020.3	23.9	28.4	1.6	633	8147	68	2423	28	
1007	1023.6	3.6	7.6	0.9	108	1261	24	3315	40	
1007	1006.5	24.9		0.7	590	8738	89	2242	26	14
1007	1048.7	9.2		0.8	1197	3711	125	2094	14	
1007	1050.3	20.7		1.1	1394	9052	98	2283	17	
1007	1056.1	12.8	26.0	1.5	547	9544	93	3350	34	20
1007	1064.4	14.7	20.5	0.6	1501	4202	218	1771	10	
1007	1069.9	12.5	22.5	0.8	955	8254	72	2650	23	18
1007	1079.1	12.6	26.9	1.0	888	3365	99	2330	21	30
1007	1096.5	22.8		0.7	1375	6987	131	2790	22	18
1007	1107.6	12.7		0.8	1513	4194	140	2310	16	16
1007	1110.7	20.4		0.6	505	4964	151	2530	13	17
1007	1110.3	13.7	25.7	0.4	787	4905	175	2720	15	19

Table 2 (continued).

Site	Depth (mbsf)	Insolubles (wt%)	Porosity (%)	Mg (%)	Fe (ppm)	Na (ppm)	Mn (ppm)	Sr (ppm)	Ba (ppm)	Li (ppm)
1007	1135.0	13.0		1.3	2886	9578	165	2620	18	24
1007	1133.6	13.2	17.4	0.3	1002	3287	171	2220	11	18
1007	1134.1	8.0	25.7	0.4	853	3950	185	2210	23	16
1007	1122.3	24.4	25.1	0.5	512	3860	109	1870	9	16
1007	1122.2	6.4	25.6	0.5	813	5829	62	1830	8	24
1007	1125.9	11.7	19.6	0.7	620	3034	85	2280	11	13
1007	1140.8	24.0	22.0	0.5	1707	7550	136	2330	9	23
1007	1140.9	9.4	22.8	0.5	1071	3789	161	2270	274	19
1007	1143.5	17.5	25.4	0.4	899	7665	124	2440	56	20
1007	1146.4	13.6	21.2	0.4	781	5923	142	2570	45	18
1007	1153.5	19.0		0.5	526	4519	139	2100	152	15
1007	1155.3	8.9	22.8	0.5	245	2613	104	1810	100	14
1007	1157.1	10.3		0.7	258	3825	89	2360	174	18
1007	1160.3	19.3	24.6	0.7	339	5107	85	1850	70	18
1007	1160.9	8.7		1.2	717	3395	69	2390	135	30
1007	1161.0	35.7	21.8	1.0	431	3884	98	2490	132	134
1007	1165.1	20.3	22.9	0.7	674	7107	136	2460	83	12
1007	1159.7	27.1		0.5	285	3399	87	1510	32	14
1007	1170.8	33.0	18.8	1.1	1334	6813	115	2190	104	20
1007	1174.3	1.1	23.2	0.6	599	3270	91	2200	103	16
1007	1177.8	16.6		0.7	623	6101	111	2100	38	16
1007	1188.7	5.6		0.6	377	4343	122	1760	119	17
1007	1190.5	0.9	5.9	0.8	709	6221	113	1800	73	18
1007	1198.2	3.3		0.5	308	3305	101	1570	147	15
1007	1206.8	1.9		0.6	347	3796	93	1800	156	13
1007	1208.2	3.1	31.6	0.6	796	5181	97	1920	95	13
1007	1216.9	10.6		0.4	289	3930	89	1810	169	14
1007	1218.1	2.3		1.3	749	9413	84	2560	104	25
1007	1228.0	2.6	30.8	0.7	632	6416	91	2290	122	16

Note: Blank cells = not measured.

elements (Cl^-, Na^+, and K^+) as well as many nonconservative elements (SO_4^{2-}, Ca^{2+}, and Mg^{2+}) are nearly vertical (Fig. 5). Below a depth of ~40 mbsf, sharp changes occur in the concentration of nearly all pore-fluid constituents and continue down to the base of the hole (Fig. 4). Slight gradients do exist in constituents of the uppermost sediments such as alkalinity, NH_4^+, and HPO_4^{2-}, which are most sensitive to small amounts of microbial degradation (Fig. 5). A review of other ODP drilling sites reveals that this type of pore-fluid shift in typically conservative elements is not a common occurrence. Three mechanisms which may contribute to the nature of these shallow profiles are examined here: (1) changing sedimentation rate or a hiatus, (2) active bottom water flushing, and (3) changing reactivity of the sediment.

Large differences in pore-fluid gradients for conservative elements like Cl^- may be explained by a sudden change in sedimentation rates, such as a period of nondeposition followed by a large input of sediment (Goldhaber and Kaplin, 1980; Aller et al., 1986). Sedimentation rates are known to have strong influences on the evolution of pore-fluid profiles by influencing the distance constituents can migrate by diffusion (Berner, 1980). Rates of sedimentation are expected to be substantially higher within the upper 20–40 mbsf if they are responsible for the vertical gradients with this zone. However, sedimentation rates based on biostratigraphic data appear nearly constant throughout the upper 100–180 m of three of the four sites, showing no hiatus or significant increase where the pore-fluid profiles change (Fig. 2). Only at Site 1007 is there a marked hiatus in deposition which roughly coincides (~40 mbsf) with the change in pore-fluid gradients (Fig. 2). Overall, sedimentation rates are higher (10–15 cm/k.y.) in the shallow intervals of the more proximal sites (Sites 1003 and 1005) compared to the more distal sites (Sites 1006 and 1007) (5 cm/k.y.). This difference in sedimentation rate may, in part, explain why the vertical pore-fluid gradients extend to a deeper depth closer to the platform margin. So whereas differences in sedimentation rates may influence the thickness of zones with vertical gradients, they fail to explain why the change in pore-fluid shift occurs where it does.

Active bottom water flushing throughout the upper 20–40 mbsf could explain the lack of significant gradients in the uppermost sediments. Bioirrigation is known to move water through fine sediments and has been documented to produce similar profiles on a much smaller scale (Aller, 1977, 1980). During Leg 166, the term "flush zone" was used to describe this shallow interval. However, no plausible mechanism was developed to explain the advection process. Although sediment dwellers typically influence the upper 1 m of sediment (Wetzel, 1981), it has been hypothesized that they influence profiles down to a depth of 8 m in high-productivity areas (Schulz et al., 1994). However, it is unlikely that bioirrigation mechanisms could produce movement of bottom water down to depths of 2040 m, particularly as both biostratigraphic and lithostratigraphic data indicate a relatively undisturbed sedimentation and the presence of semilithified horizons and hardgrounds (Eberli, Swart, Malone, et al., 1997). A more plausible mechanism to advect bottom water through these upper sediments would involve the strong bottom currents that sweep the western slope of the Bahamas Bank and which may have been active since the late Pliocene. Studies of the Florida Current around 27°N indicate bottom currents with velocities in the 10–20 cm/s range (Wang and Mooers, 1997). Whereas bottom currents are not known within the Santaren Channel, the overall flow through the channel is roughly 10% that of the Florida Current. By extension, Santaren bottom currents might be expected to have velocities in the 1–2 cm/s range. Currents in this range could be strong enough to entrain pore-fluids and rework surface sediments. This could have the effect of (1) enhancing exchange of pore-fluids with oxygenated bottom water and (2) increasing the degree of organic matter destruction prior to sediment burial.

A third explanation for the absence of significant chemical gradients in the upper 40 mbsf is that the upper sediments are simply less reactive compared to the sediments below. There is fairly good evidence that the upper sediments down to 20–40 mbsf are oxic to suboxic, following a depth succession of deoxygenation and denitrification. Narrow zones near ~10 mbsf at both Sites 1005 and 1003 show small but significant increases in alkalinity, NH_4^+, and HPO_4^{2-}, but no changes in SO_4^{2-}, indicating small amounts of organic matter oxidation probably by NO_3^- reduction (Fig. 5). Incubation tests done onboard *JOIDES Resolution* on samples taken from above 30 mbsf at Site 1007 showed no substantial change in pore-fluid constituents after 60 hr, supporting the idea that sediment reactivity is fairly low (P. Kramer and N. Schovsbo, unpubl. data). The lack of reactivity in the uppermost sediments could result from a change in sediment character (labile organic carbon, mineralogy, or grain size) compared to the sediments below. Shipboard lithostratigraphic data do not indicate a

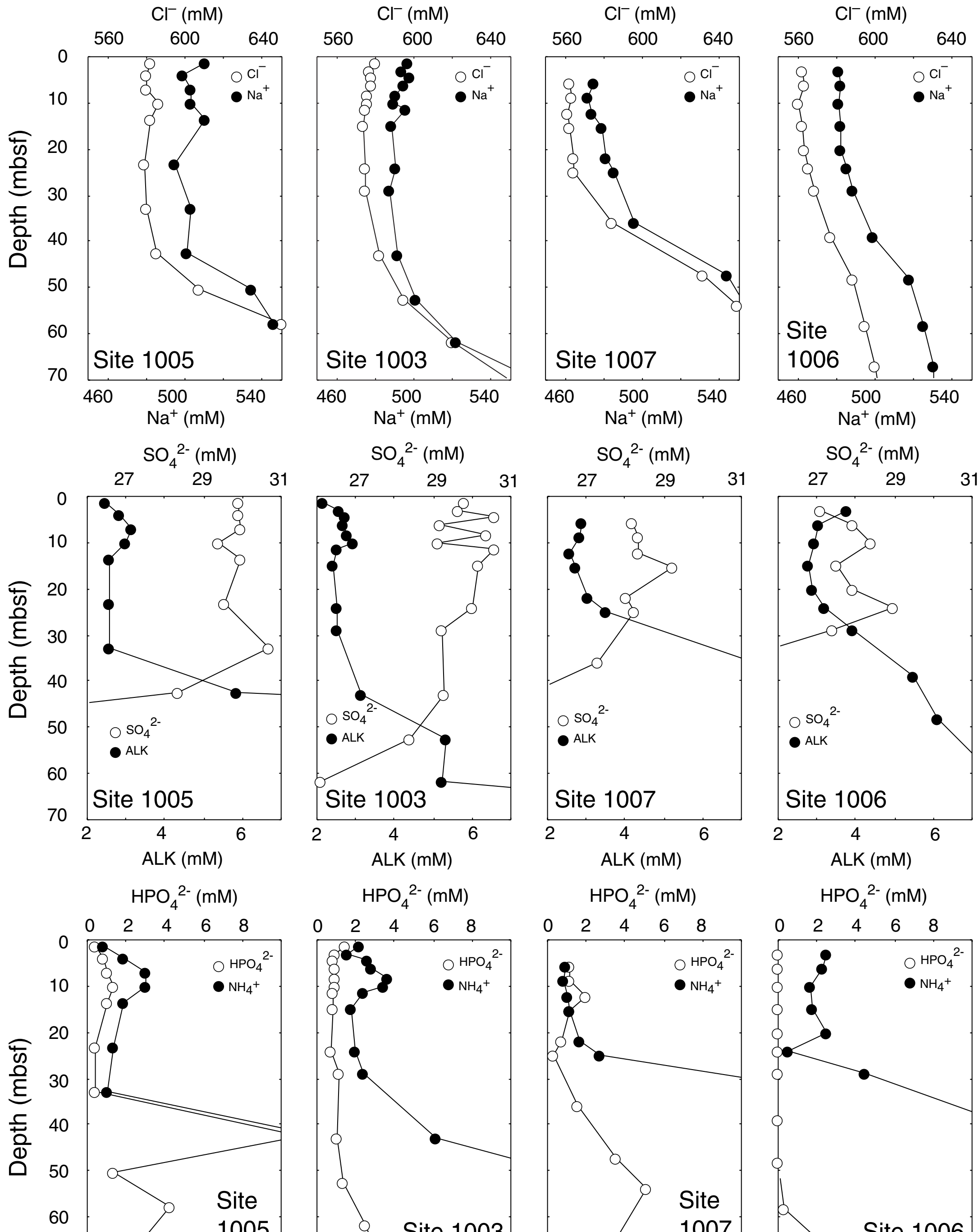

Figure 5. Expanded depth profiles of selected interstitial water constituents for the upper 70 mbsf of Sites 1006, 1007, 1003, and 1005 showing shifts between 20 and 40 mbsf. ALK = alkalinity.

major change in the sediment grain size or mineralogy through the interval where the pore-fluid shift occurs, although partly lithified horizons of HMC are more common below 40 mbsf. Total organic carbon (TOC) concentrations do appear to increase below 40 mbsf, particularly at Sites 1003–1005 (Fig. 2). This would suggest that increases in organic content may cause a shift in sediment reactivity, which is reflected in many of the nonconservative pore-fluid constituents (SO_4^{2-}, alkalinity, NH_4^+, PO_4^{2-}, Ca^{2+}, Mg^{2+}, and Sr^{2+}). It may also explain the shift seen in Cl^- and Na^+ contents if these elements are not behaving conservatively, as is explored in the next section.

Cl^- and Na^+ Profiles

Large (up to two-fold) increases in dissolved Cl^- and Na^+ concentrations from present bottom-water composition occur throughout the Bahamas Transect below 40 mbsf (Fig. 4). The largest gradients occur near the platform margin, whereas the smallest gradients are found at the more distal sites. The possibility that the higher salinity pore fluids were emplaced by fluid-flow advection of brines from deeper sequences is not likely for two reasons. First, the isotopic composition of dissolved strontium ($^{87}Sr/^{86}Sr$) in pore fluids at Sites 1003–1007 is in equilibrium with the contemporaneous seawater curve throughout the Pliocene–Miocene sediments (P. Swart and H. Elderfield, unpubl. data). Second, throughout the Pliocene–Miocene sections, pore-fluid constituents are dominated by diffusional gradients and appear to be in equilibrium with the surrounding sediments. For example, within Sites 1003 and 1005, celestite ($SrSO_4$) is mainly found in core intervals high in dissolved SO_4^{2-} and saturated with respect to celestite. At Site 1007, pore-fluid Ba^{2+} concentrations are elevated only in the lower intervals where significant amounts of sedimentary acid-soluble barite are present (Fig. 6). This implies that Leg 166 pore fluids are probably in situ and have evolved to their present composition through interaction with the surrounding sediments and diffusion.

Increases observed in pore-fluid Cl^- and Na^+ concentrations with depth along the Bahamas Transect are a relatively common occurrence along continental and bank margins. During Leg 101, a series of shallow (~<400 mbsf) holes throughout the Bahamas archipelago were drilled and similar increases in salinity at many of the sites were found (Austin, Schlager, Palmer, et al., 1986). During Leg 133, periplatform carbonate sediments drilled off the northeastern coast of Australia revealed a substantial increase in Cl^- at Sites 715 and 823; the increase was interpreted to be caused by diffusion from an underlying evaporite unit (Davies, McKenzie, Palmer-Julson, et al., 1991). Similarly, Leg 150 scientists interpreted the nearly twofold increases in Cl^- and Na^+ content to result from upward diffusion of deeply buried Jurassic salt along the New Jersey Margin (Miller and Mountain, 1994). Triassic to Lower Jurassic sediments underlying the Bahamas/Florida region are thought to contain evaporites (Sheridan, 1974), and deep salt diapirs are evident on seismic profiles further south. Therefore, it is likely that at Sites 1003–1007 some of the increase in salinity with depth may be caused by upward diffusion of Cl^- and Na^+. However, an examination of pore-fluid Na^+/Cl^- ratios shows no significant trend with depth from bottom-water ratios (0.86) except at Site 1006, where there is probably a high degree of clay-mineral interactions involving Na^+ (Fig. 7). The pore-fluid $\delta^{18}O$ data do show an increase by nearly 2.5‰ at the base of Sites 1003 and 1007, but this increase is interpreted to reflect influences of carbonate recrystallization rather than the influence of an enriched, deep-seated brine or evaporites (Swart, Chap. 8, this volume). In addition, it is not easy to explain how diffusion alone would cause the marked differences in concentration gradients for Na^+ and Cl^- along the transect (Fig. 4). For example, at Site 1005 Cl^- concentrations increase to 796 mM at a depth of 122.4 mbsf, then decrease to 742 mM at a depth of 178 mbsf, all within Pleistocene sediments. At Site 1006, this range of Cl^- concentration is not reached until a depth of ~453 mbsf within Miocene sediments.

Here, it is postulated that another possible source for the increased Na^+ and Cl^- concentrations with depth might be salt inclusions contained within defects of the biogenic aragonite, HMC carbonate structure. During diagenetic recrystallization of LMC and dolomite, these salt inclusions may be excluded into the pore water. This process was documented by Malone et al. (1990) at Site 716 in the Maldives archipelago. In this case, sediments originally composed of ~25% aragonite and HMC decreased in sodium content by ~1200 ppm as a result of conversion to LMC over a period of 2.5 Ma. The effect on pore-fluid Na^+ content cannot be determined because this constituent was not analyzed, but dissolved Cl^- does show some localized increases, although no systematic trend is evident.

A rough calculation can be made to determine the possible influence of sodium expulsion on pore-water concentrations. Sodium concentrations are known to be enriched in biogenic aragonite and HMC

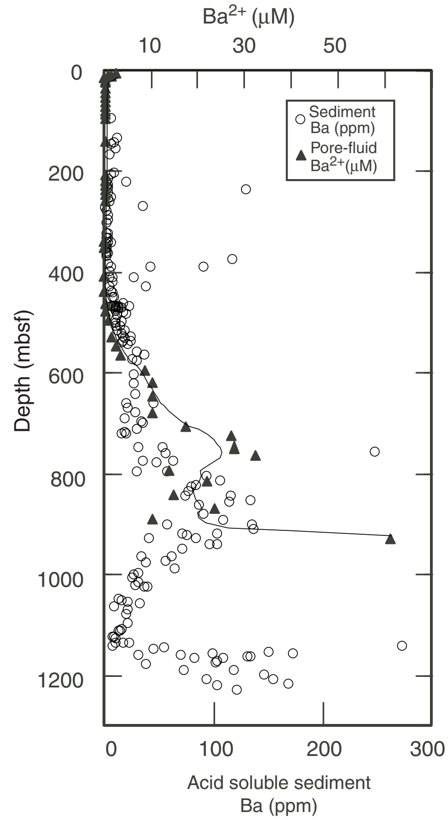

Figure 6. Depth profiles of pore-fluid dissolved Ba^{2+} concentration and barium concentration measured in the acid soluble fraction of Site 1007 sediments.

compared to LMC (foraminifers and coccoliths) (Busenberg and Plummer, 1985). Sodium concentrations are ~4000 ppm in aragonite, whereas they are much lower in LMC (~500 ppm) (Milliman, 1974). Assuming sediments are originally 100% aragonite containing 4000 ppm sodium, complete recrystallization to 500 ppm LMC could release enough sodium to raise pore-fluid concentrations by nearly 1.5 × seawater values. Sediment porosity values can be used as a proxy indicator for the degree of carbonate recrystallization. An examination of the solid-phase data from Sites 1005 and 1007 shows that sodium concentration and sediment porosity are well correlated, particularly in samples with <30% porosity (Fig. 8). Sodium values are higher than expected, particularly for high-porosity samples, and much of the scatter probably results from incomplete removal of dried salts during sample preparation. However, the well-defined trend in samples with <30% porosity seems to support the idea that, as biogenic carbonates are recrystallized, sodium (and presumably chloride) are expelled from the mineral structure, which should cause small increases in pore-fluid salinity. This process would certainly explain why there are larger (and steeper) gradients in Cl^- and Na^+ near the platform margin (Site 1005), where carbonate recrystallization is more prevalent compared to the more distal sites. It could also explain why shifts around 20–40 mbsf in Cl^- and Na^+ contents coincide with shifts seen in other pore-fluid constituents influenced by carbonate remineralization such as Sr^{2+}.

Carbonate Diagenesis

Lithostratigraphy and mineralogy results indicate that all sites examined along the Bahamas Transect are heavily influenced by carbonate recrystallization. In general, the more proximal sites show a

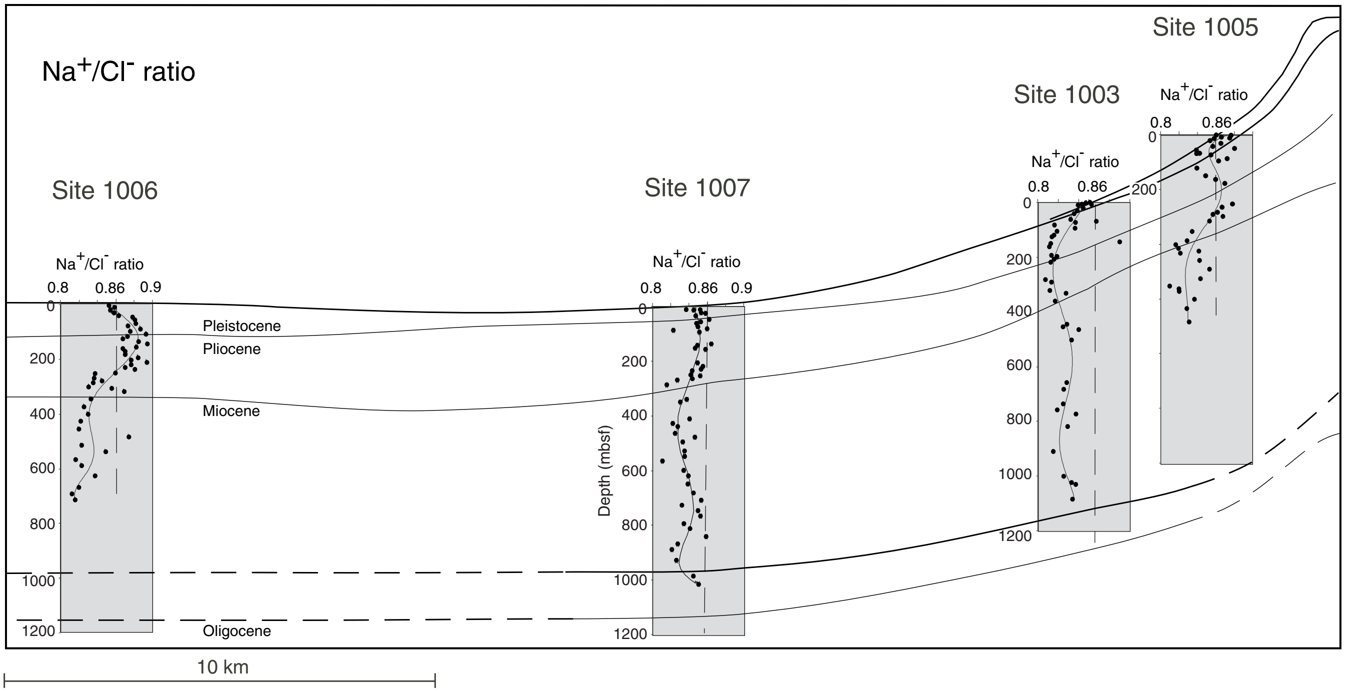

Figure 7. Depth profile of Na^+/Cl^- ratios superimposed on an interpreted seismic section for Sites 1006, 1007, 1003, and 1005.

higher degree of diagenetic carbonate alteration than the more distal sites (Eberli, Swart, Malone, et al., 1997). This higher degree of alteration probably results from the fact that the diagenetic potential is higher along the platform margin as a result of (1) higher input of metastable carbonate and organic matter during highstands along the platform margin, and (2) decreased influence of clay minerals. The chemistry of interstitial waters below 40 mbsf also indicates extensive carbonate alteration, principally aragonite dissolution and calcite and dolomite precipitation.

All sites show a large increase (up to 70-fold) in dissolved Sr^{2+} derived from the recrystallization of metastable aragonite to LMC. Strontium concentrations are much higher in aragonite (12,000 ppm) than LMC (2000 ppm) (Milliman, 1974). The amount of Sr^{2+} able to remain in solution is largely controlled by the solubility of celestite ($SrSO_4$) and, therefore, can only be used as a measure of the degree of carbonate alteration when pore-fluid SO_4^{2-} concentrations are very low or absent (Baker and Bloomer, 1988; Swart and Guzakowski, 1988). A plot of Cl^- vs. Sr^{2+} for all sites shows that the two are well correlated at Site 1006, the only site where SO_4^{2-} is absent from pore fluids below 200 mbsf and where no celestite was detected in the cores (Fig. 9). Again, this seems to support the idea that dissolved chloride and sodium are influenced by carbonate remineralization.

Dolomite formation is also an important diagenetic process occurring within sediments below 40 mbsf along the Bahamas Transect. The largest increases in the Mg^{2+}/Ca^{2+} ratios appear to coincide with intermediate-depth intervals (50–200 mbsf), where extensive sulfate reduction is occurring (Fig. 10) Within these intervals, the Mg^{2+}/Ca^{2+} ratios increase on the order of 1:3 suggesting dolomite formation by recrystallization of aragonite and HMC (Baker and Kastner, 1981). Significant dolomite (up to 20%) was detected in the upper Pliocene–Pleistocene sediments near sequence boundaries (Fig. 3). In lower sediment regimes (middle Pliocene–Miocene units), there is a progressive loss of Mg^{2+} and increase in Ca^{2+} concentrations leading to a decrease in the Mg^{2+}/Ca^{2+} ratios (Fig. 10). Small amounts of dolomite (background dolomite) are probably forming throughout these intervals but are limited by the availability of Mg^{2+} supplied by carbonate recrystallization and diffusion from the overlying seawater.

Organic Matter Diagenesis

Pore-fluid chemistry and headspace analyses indicate that the remineralization of organic matter is an important process along the Bahamas Transect. Oxidation of organic matter by sulfate reduction is evident at all sites below 40 mbsf, based on the presence of H_2S gas (Eberli, Swart, Malone et al., 1997). Sulfate reduction is most pronounced in the shallow Pliocene–Recent intervals close to the platform margin, where high rates of sedimentation (15 cm/k.y.) result in the burial of substantial quantities of organic material (Fig. 2). At Site 1005, sulfate content is reduced and below the limits of detection (~1 mM) by a depth of 87 mbsf (Fig. 4). The concomitant increase in alkalinity within this zone of sulfate depletion follows a 2:1 ratio (i.e., a 2-mole increase in total alkalinity per one mole of sulfate lost), which agrees with the predicted model of microbial sulfate reduction (Berner, 1971). What is unusual about Site 1005 (along with Sites 1003 and 1007) is that rather than remain depleted, dissolved SO_4^{2-} *increases* in excess of bottom-water concentrations (30 mM) below this zone of sulfate reduction (Fig 4). This alternation between sulfate-reducing and non–sulfate-reducing zones is very unusual and is examined in more detail below.

Sulfate reduction is normally limited by the availability of labile organic matter and dissolved SO_4^{2-}. Therefore, we might expect that sulfate-reducing intervals should have a higher abundance of labile organic matter compared to non–sulfate-reducing intervals. An examination of Figure 2 for Sites 1003 and 1005 shows a rough correspondence, but more samples need to be analyzed to test this hypothesis. The availability of dissolved SO_4^{2-} in deeper sequences (>200 mbsf) is believed to be largely limited by the presence of available dissolved Fe^{2+}. Dissolved Fe^{2+} will sequester reduced sulfate (HS^-) to form sedimentary pyrite (Berner, 1966; Canfield, 1989). Significant amounts of pyrite were observed at Sites 1006 and 1007 and below 1070 mbsf at Site 1003. The origin of the dissolved Fe^{2+} is believed to be from Fe-Mn–rich phases associated with siliciclastic clays (smectite, feldspar, quartz, and kaolinite) deposited by channel currents at the more distal sites (Eberli, Swart, Malone, et al., 1997). In contrast, Site 1005 and intervals of Site 1003 probably receive only

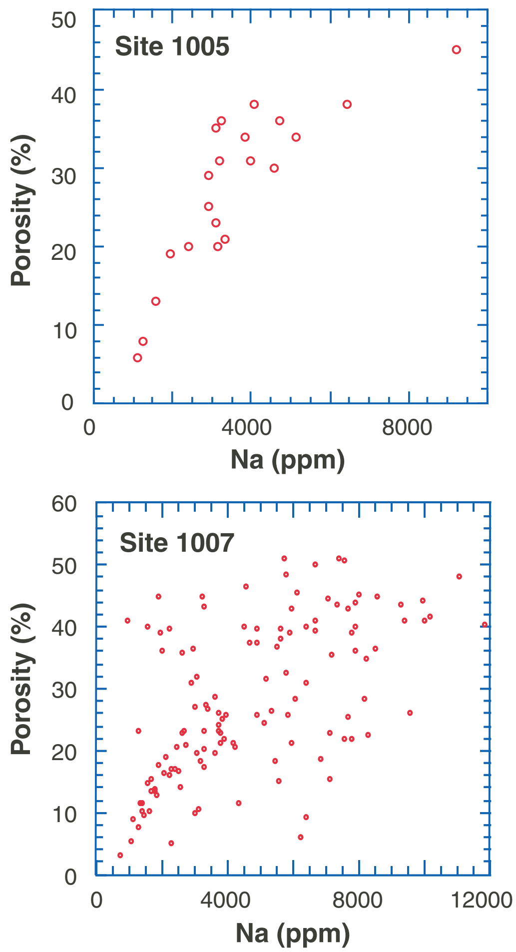

Figure 8. Relationship between sodium concentrations and bulk porosity for acid soluble sediments analyzed from Sites 1005 and 1007. The decrease in sodium concentration with decreasing porosity is postulated to result from the expulsion of sodium from the crystal structure during carbonate recrystallization.

minimal fluxes of Fe^{2+} delivered by detrital mineral phases and, correspondingly, show only trace levels of iron-sulfide formation. Sulfide produced by SO_4^{2-} reduction is built up to high concentrations thereby reducing the sediment pH (Ben-Yaakov, 1973). As levels of free hydrogen-sulfide continue to build up in the interstitial waters, reaction pathways are dominated by the oxidation of elemental sulfur back to sulfate, which further reduces the pH (Goldhaber and Kaplan, 1980; Aller, 1982). This results in enhanced carbonate dissolution (Canfield and Raiswell, 1991) and may explain why the platform margin sediments are much more reactive in terms of carbonate recrystallization than the sediments of the more distal sites. Once all labile organic material is oxidized, sulfate reduction is inhibited and all reduced forms of sulfide are gradually transformed back to dissolved SO_4^{2-}, which can remain at high concentrations.

Therefore, the combined influences of availability of labile organic carbon and dissolved Fe^{2+} are believed to control the alternations between sulfate-rich and sulfate-depleted zones. Diffusion of constituents from above and below these boundaries leads to the formation of many diagenetic sulfur minerals at these interfaces, such as barite, celestite, and elemental sulfur. Figure 11 shows Sr^{2+} and SO_4^{2-} profiles for Site 1007 illustrating where celestite is forming as waters become saturated with respect to this mineral.

Degradation of organic matter by methane oxidation is also an important process along the Bahamas Transect. The high concentration of methane gas detected within the Pleistocene–Pliocene intervals of Sites 1003–1005 indicates that oxidation of organic matter by methane is occurring immediately below the sulfate-reduction zones. The peak concentrations of NH_4^+ are commonly below the alkalinity maximum and below the base of the sulfate-reduction zone, as has been observed in other settings where methanogenesis is an important process (Mackin and Aller, 1984). It is also highly probable that partial sulfate reduction may also be occurring by oxidation of upwardly migrating methane (Burns, 1998).

An examination of the pore-fluid $\delta^{13}C$ of the DIC shows behavior similar to other carbonate-dominated sites where sulfate reduction and methanogenesis occur (Swart, 1993). While DIC $\delta^{13}C$ profiles reflect these processes, they are strongly buffered by the host carbonate and consequently only display minor changes in the $\delta^{13}C$. Surprisingly, one of the regions displaying the most negative $\delta^{13}C$ values is the upper nonreactive zone, supporting the idea that, whereas there may be small amounts of organic matter oxidation using oxygen, there is little carbonate diagenesis taking place. Near the base of the flush zone (20–40 mbsf), all DIC $\delta^{13}C$ values increase slightly to between +1‰ and +1.5‰, then show a decrease to a minimum of –1.2‰ at Site 1005, –0.8‰ at Site 1004, and +0.81‰ at Site 1003 correspond-

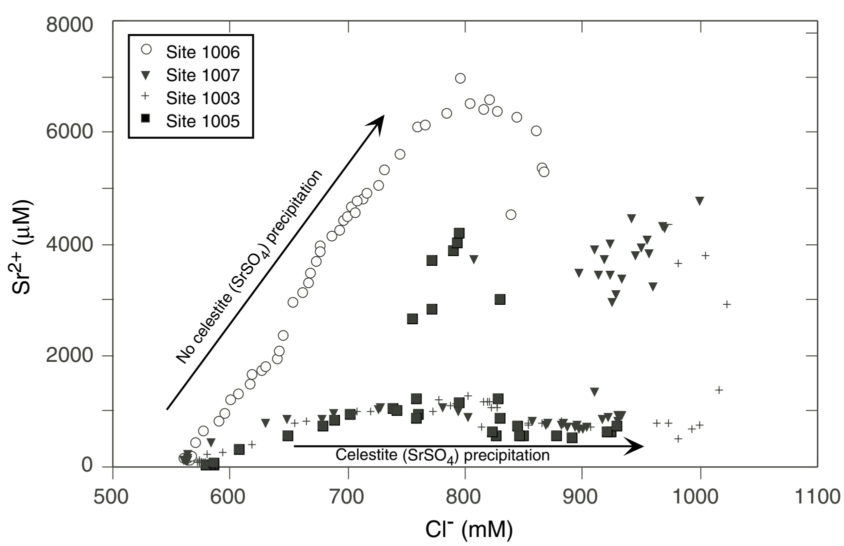

Figure 9. Plot of pore-fluid Cl^- vs. Sr^{2+} for Sites 1006, 1007, 1003, and 1005. The good correlation at Site 1006 is interpreted to illustrate the influence of carbonate recrystallization on both constituents in the absence of celestite ($SrSO_4$) formation.

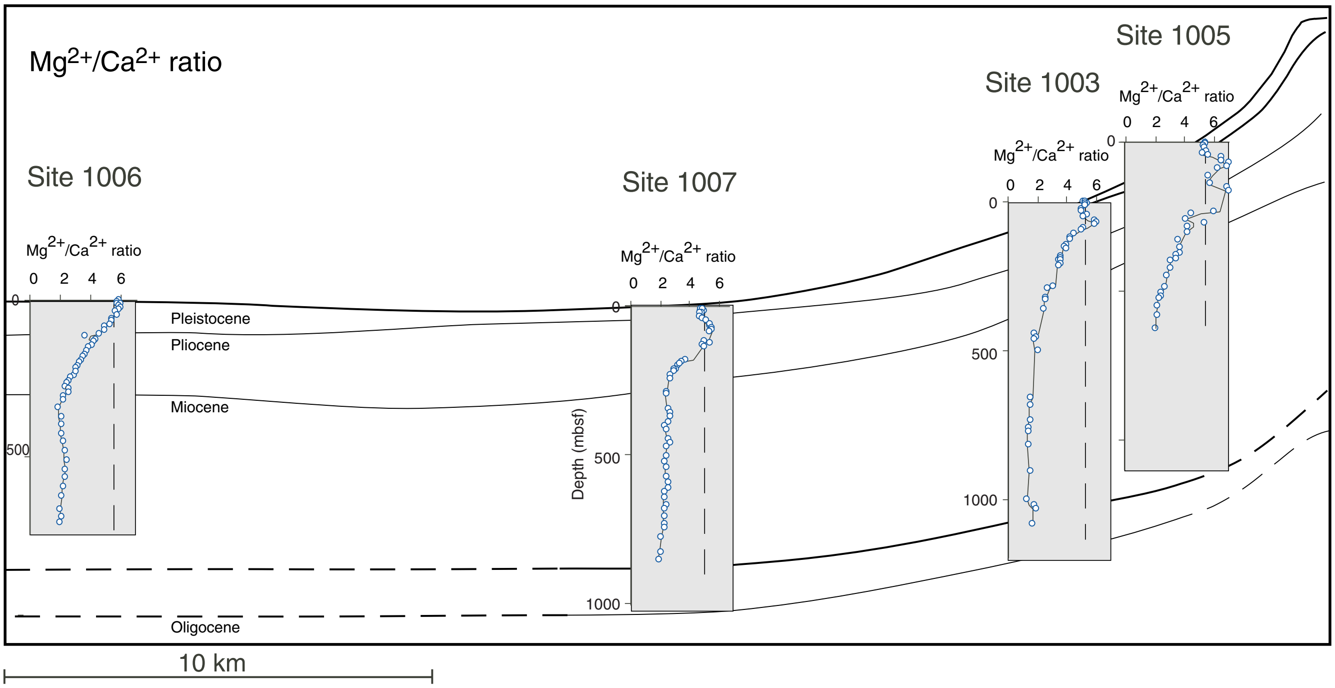

Figure 10. Depth profile of Mg^{2+}/Ca^{2+} ratios superimposed on an interpreted seismic section for Sites 1006, 1007, 1003, and 1005. Dolomite formation is most favored in shallow areas where extensive sulfate reduction and carbonate dissolution leads to high Mg^{2+}/Ca^{2+} ratios.

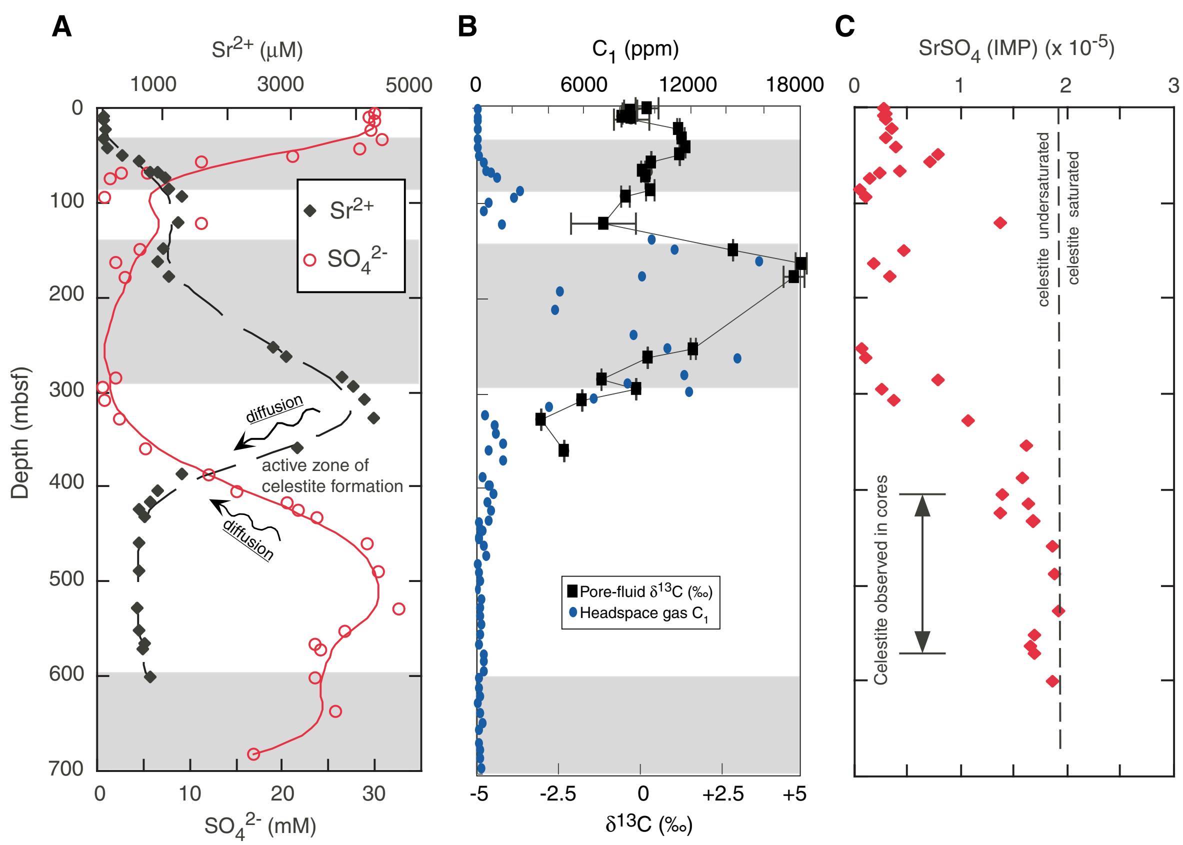

Figure 11. Site 1005 depth profiles illustrating altenations between sulfate-reducing (shaded) and non–sulfate-reducing zones. Interfaces between these zones are important sites of dissolution/precipitation reactions. **A.** SO_4^{2-} and Sr^{2+}. **B.** Methane (C_1) measured in headspace and interstitial dissolved inorganic carbon (DIC) $\delta^{13}C$. **C.** Ion molar product (IMP) for celestite ($SrSO_4$) and interval (indicated by arrows) where significant quantities of celestite were found in cores.

ing to the loss of SO_4^{2-}. Although this minimum reflects an increasing contribution from the oxidation of organic material by sulfate, it is masked by the input of carbon from the dissolution of carbonate. The $\delta^{13}C$ values increase with increasing depth, perhaps reflecting equilibration with CO_2 produced during methanogenesis. At Site 1005, the $\delta^{13}C$ values decrease with increasing depth reflecting the reduced influence of methanogenesis below 300 mbsf (Fig. 10).

CONCLUSIONS

1. The shallow, vertical pore-water gradients observed along the Bahamas Transect are thought to be influenced primarily by differences in sediment reactivity, possibly induced by changes in sedimentation rates and strong bottom currents active since the late Pliocene.
2. Pore-fluid profiles in the lower Pliocene–Miocene sequences are dominated by diffusion and do not show significant evidence of subsurface advective flow. Deeper interstitial waters are believed to be the in situ fluids that have evolved mainly through interactions with sediments.
3. The increase in Na^+ and Cl^- content observed with depth is postulated to result from the expulsion of Na^+ and Cl^- into pore waters during alteration of metastable aragonite and HMC to LMC and dolomite. It is also possible that some of the increase is caused by upward diffusion of salt from Early Jurassic evaporites.
4. Pore-fluid chemistry is dominated by the influences of carbonate recrystallization, much of which is thought to occur soon after deposition during open exchange with bottom water. Extensive later stage burial diagenesis of carbonate is limited to zones of sulfate-reduction reactions, where enhanced carbonate dissolution occurs.
5. Marginal sites are characterized by alternations between sulfate-reducing and non–sulfate-reducing zones, which are controlled by the availability of labile organic matter and sulfate. Sulfate availability in deeper sediments is controlled by sulfur cycling pathways and the presence or absence of dissolved Fe^{2+}. Interfaces between sulfate-reducing and non–sulfate-reducing zones are sites of ongoing reaction and precipitation of minerals such as celestite and barite.

ACKNOWLEDGMENTS

The authors would like to thank the technicians, scientists, and crew of Leg 166 for their assistance during the cruise. T. Bronk and A. Pimmel are especially thanked for their help in the chemistry lab. J. Robinson assisted with portions of the solid-phase analyses. F. Anselmetti and J. Kenter are thanked for providing bulk-porosity data. We thank Steve Burns, John Compton, and Mitch Malone for comments and suggestions that improved an earlier version of this manuscript. Portions of this research were supported by grants from JOI/USSAC (PAK, PKS, and EHD).

REFERENCES

Aller, R.C., 1977. The influence of macrobenthos on chemical diagenesis of marine sediments [Ph.D. dissertation]. Yale Univ.

————, 1980. Quantifying solute distribution in the bioturbated zone of marine sediments by defining an average microenvironment. *Geochim. Cosmochim. Acta,* 44:1955–1965.

————, 1982. Carbonate dissolution in nearshore terrigenous muds: the role of physical reworking. *J. Geol.,* 90:79–95.

Aller, R.C., Mackin, J.E., and Cox, R.T., 1986. Diagenesis of Fe and S in Amazon inner shelf muds: apparent dominance of Fe reduction and implications for the genesis of ironstones. *Cont. Shelf Res.,* 6:263–289.

Austin, J.A., Jr., Schlager, W., Palmer, A.A., et al., 1986. *Proc. ODP, Init. Repts.,* 101: College Station, TX (Ocean Drilling Program).

Baker, P.A., and Bloomer, S.H., 1988. The origin of celestite in deep-sea carbonate sediments. *Geochim. Cosmochim. Acta,* 52:335–339.

Baker, P.A., and Kastner, M., 1981. Constraints on the formation of sedimentary dolomite. *Science,* 213:215–216.

Ben-Yaakov, S., 1973. pH buffering of pore waters of recent anoxic marine sediments. *Limnol. Oceanogr.,* 18:86–94.

Berner, R.A., 1966. Chemical diagenesis of some modern carbonate sediments. *Am. J. Sci.,* 264:1–36.

Berner, R.A., 1971. *Principles of Chemical Sedimentology:* New York (McGraw-Hill).

Berner, R.A., 1980. *Early Diagenesis: A Theoretical Approach:* Princeton, NJ (Princeton Univ. Press).

Burns, S.J., 1998. Carbon isotopic evidence for coupled sulfate reduction-methane oxidation in Amazon Fan sediments. *Geochem. Cosmochim. Acta,* 62:797–804.

Busenberg, E., and Plummer, L.N., 1985. Kinetic and thermodynamic factors controlling the distribution of SO_4^{2-} and Na^+ in calcites and selected aragonites. *Geochem. Cosmochim. Acta,* 49:713–725.

Canfield, D.E., 1989. Reactive iron in marine sediments. *Geochem. Cosmochim. Acta,* 53:619–632.

Canfield, D.E., and Raiswell, R., 1991. Pyrite formation and fossil preservation. *In* Allison, P.A., and Briggs, D.E.G. (Eds.), *Topics in Geobiology* (Vol. 9): *Taphonomy: Releasing the Data from the Fossil Record:* New York (Plenum Press), 337–387.

Cranston, R.E., and Buckley, D.E., 1990. Redox reactions and carbonate preservation in deep-sea sediments. *Mar. Geol.,* 94:1–8.

Davies, P.J., McKenzie, J.A., Palmer-Julson, A., et al., 1991. *Proc. ODP, Init. Repts.,* 133 (Pts. 1, 2): College Station, TX (Ocean Drilling Program).

Eberli, G.P., Swart, P.K., Malone, M.J., et al., 1997. *Proc. ODP, Init. Repts.,* 166: College Station, TX (Ocean Drilling Program).

Gieskes, J.M., Gamo, T., and Kastner, M., 1993. Major and minor element geochemistry of interstitial waters of Site 808, Nankai Trough: an overview. *In* Hill, I.A., Taira, A., Firth, J.V., et al., *Proc. ODP, Sci. Results,* 131: College Station, TX (Ocean Drilling Program), 387–396.

Goldhaber, M.B., and Kaplan, I.R., 1980. Mechanisms of sulfur incorporation and isotope fractionation during early diagenesis in sediments of the Gulf of California. *Mar. Chem.,* 9:95–143.

Kastner, M., Elderfield, H., Martin, J.B., Suess, E., Kvenvolden, K.A., and Garrison, R.E., 1990. Diagenesis and interstitial-water chemistry at the Peruvian continental margin—major constituents and strontium isotopes. *In* Suess, E., von Huene, R., et al., *Proc. ODP, Sci. Results,* 112: College Station, TX (Ocean Drilling Program), 413–440.

Kitano, Y., Okumaura, M., and Idogak, M., 1978. Uptake of phosphate ions by calcium carbonate. *Geochem. J.,* 12:29–37.

Mackin, J.E., and Aller, R.C., 1984. Ammonium adsorption in marine sediments. *Limnol. Oceanogr.,* 29:250–257.

Malone, M.J., Baker, P.A., Burns, S.J., and Swart, P.K., 1990. Geochemistry of periplatform carbonate sediments, Leg 115, Site 716 (Maldives Archipelago, Indian Ocean). *In* Duncan, R.A., Backman, J., Peterson, L.C., et al., *Proc. ODP, Sci. Results,* 115: College Station, TX (Ocean Drilling Program), 647–659.

Miller, K.G., and Mountain, G.S., 1994. Global sea-level change and the New Jersey margin. *In* Mountain, G.S., Miller, K.G., Blum, P., et al., *Proc. ODP, Init. Repts.,* 150: College Station, TX (Ocean Drilling Program), 11–20.

Milliman, J.D., 1974. *Marine Carbonates* (2nd ed.): Berlin (Springer-Verlag).

Schulz, H.D., Dahmke, A., Schinzel, U., Wallmann, K., and Zabel, M., 1994. Early diagenetic processes, fluxes, and reaction rates in sediments of the South Atlantic. *Geochim. Cosmochim. Acta,* 58:2041–2060.

Sheridan, R.E., 1974. Atlantic continental margin of North America. *In* Burk, C.C., and Drake, C.L. (Eds.), *Geology of Continental Margins:* New York (Springer Verlag), 391–407.

Swart, P.K., 1993. The formation of dolomite in sediments from the continental margin of northeastern Queensland. *In* McKenzie, J.A., Davies, P.J., Palmer-Julson, A., et al., *Proc. ODP, Sci. Results,* 133: College Station, TX (Ocean Drilling Program), 513–523.

Swart, P.K., and Guzikowski, M., 1988. Interstitial-water chemistry and diagenesis of periplatform sediments from the Bahamas, ODP Leg 101. *In* Austin, J.A., Jr., Schlager, W., Palmer, A.A., et al., *Proc. ODP, Sci. Results,* 101: College Station, TX (Ocean Drilling Program), 363–380.

Swart, P.K., Isern, A., Elderfield, H., and McKenzie, J.A., 1993. A summary of interstitial-water geochemistry of Leg 133. *In* McKenzie, J.A., Davies, P.J., Palmer-Julson, A., et al., *Proc. ODP, Sci. Results,* 133: College Station, TX (Ocean Drilling Program), 705–721.

Wang, J., and Mooers, C.N.K., 1997. Three-dimensional perspectives of the Florida Current: transport, potential velocity, and related dynamical properties. *Dyn. Atmosph. Oceans,* 27:135–149.

Wetzel, A., 1981. Ökologische und stratigraphische Bedeutung biogener Gefüge in quartären Sedimenten am NW-afrikanischen Kontinentalrand. *"Meteor" Forschungsergeb. Reihe C,* 34:1–34.

Date of initial receipt: 29 March 1999
Date of acceptance: 16 August 1999
Ms 166SR-117